Sea-ice transport driving Southern Ocean salinity and its recent trends

Author(s):
Haumann, Alexander; Gruber, Nicolas; Münnich, Matthias; Frenger, Ivy; Kern, Stefan

Publication date:
2016-09

Permanent link:
https://doi.org/10.3929/ethz-b-000120143

Originally published in:
Nature 537(7618), https://doi.org/10.1038/nature19101

Sea-ice transport driving Southern Ocean salinity and its recent trends

F. Alexander Haumann[*1,2], Nicolas Gruber[1,2], Matthias Münnich[1], Ivy Frenger[1,3], Stefan Kern[4]

[1]Environmental Physics, Institute of Biogeochemistry and Pollutant Dynamics, ETH Zürich, Universitätstrasse 16, 8092 Zürich, Switzerland

[2]Center for Climate Systems Modeling, ETH Zürich, Universitätstrasse 16, 8092 Zürich, Switzerland

[3]Biogeochemical Modelling, GEOMAR Helmholtz Centre for Ocean Research Kiel, Düsternbrooker Weg 20, 24105 Kiel, Germany

[4]Integrated Climate Data Center - ICDC, Center for Earth System Research and Sustainability, University of Hamburg, Hamburg, Germany

Recent salinity changes in the Southern Ocean[1–7] are among the most prominent signals in the global ocean, yet their underlying causes have not been firmly established[1,3,4,6]. Here, we propose that trends in northward transport of Antarctic sea ice are a major contributor to these changes. Using satellite observations supplemented by sea-ice reconstructions, we estimate that the wind-driven[8,9] northward freshwater transport by sea ice increased by 20±10% between 1982 and 2008. The strongest and most robust increase occurred in the Pacific sector coinciding with the largest observed salinity changes[4,5]. We estimate that the additional freshwater for the entire northern sea-ice edge entails a freshening rate of −0.02±0.01 g kg^{-1} per decade in open ocean surface and intermediate waters, similar to the observed freshening[1–5]. The enhanced rejection of salt near the coast of Antarctica associated with stronger sea-ice export counteracts regionally the freshening of continental shelf[2,10,11] and newly formed bottom waters[6] due to the increasing addition of glacial meltwater[12]. Although the data sources underlying our results have substantial uncertainties, regional analyses[13] and independent data from an atmospheric reanalysis support our conclusions. Our finding that northward sea-ice freshwater transport is a key determinant of the Southern Ocean salinity distribution also in the mean state further underpins the importance of the sea-ice induced freshwater flux. Through its influence on the ocean's density structure[14], this process has critical consequences for the global climate by affecting the deep-to-surface ocean exchange of heat, carbon, and nutrients[14–17].

Manuscript published as:

Haumann, F., Gruber, N., Münnich, M. et al. Sea-ice transport driving Southern Ocean salinity and its recent trends. Nature 537, 89–92 (2016). https://doi.org/10.1038/nature19101.

Observations of salinity in the Southern Ocean over the last decades have revealed a substantial, wide-spread freshening in both coastal[10,18] and open ocean surface waters[2,5] as well as in the water masses sourced from these regions[1,3,4,6]. In particular, Antarctic Intermediate Water (AAIW) and Subantarctic Mode Water (SAMW) freshened at a rate between −0.01 and −0.03 g kg^{-1} per decade during the second half of the 20th century[1,3,4]. In the Pacific and Indian Ocean sectors, continental shelf waters and Antarctic Bottom Water (AABW) also freshened substantially[2,6,10], while in the Atlantic this freshening was smaller[6,18]. These salinity changes have been attributed to increased surface freshwater fluxes, stemming either from enhanced Antarctic glacial melt[2,6,10–12] or from increased atmospheric freshwater fluxes, as a result of an excess of precipitation over evaporation[1,5]. Glacial meltwater[12] most likely freshened coastal waters in the Amundsen and Ross Seas[2,10,11], but the freshening signal in AABW, which is formed in this region, is much smaller than expected[6]. In contrast, in the open Southern Ocean, increases in the atmospheric freshwater flux as simulated by global climate models appear to be largely insufficient to explain the recent freshening of AAIW[1,4].

Changes in northward sea-ice transport could possibly contribute to the wide-spread salinity changes in the Southern Ocean[8]. This process acts as a lateral conveyor of freshwater by extracting freshwater from the coastal regions around Antarctica where sea ice forms and releasing it at the northern sea-ice edge where sea ice melts[19–21] (Figure 1a). Despite substantial wind-driven changes in sea-ice drift over the last few decades[8,9], this contribution has not been quantified yet. Here, we suggest that surface freshwater fluxes induced by a stronger northward sea-ice transport are a major cause for the observed salinity changes in recent decades. The large contribution of freshwater transport by sea ice to the salinity trends is corroborated by our finding that this process plays a key role for the climatological mean salinity distribution.

Our conclusions are based on basin-scale estimates of annual net sea-ice-ocean freshwater fluxes and annual northward transport of freshwater by sea ice over the period 1982 through 2008. Further evidence in support is provided by our assessment of atmospheric reanalysis data[22] and results from another regional study[13]. We derived the sea-ice related freshwater fluxes by combining sea-ice concentration, drift, and thickness data and by using a mass-balance approach of the sea-ice volume divergence and local change (Methods). The analysed sea-ice concentration stems from satellite observations[23] (Extended Data Figure 1) and its thickness from a combination of satellite data[24] and a model-based sea-ice reconstruction that assimilates satellite data[25] (Extended Data Figure 2). The sea-ice volume divergence was computed from satellite-based sea-ice drift vectors[26] (Extended Data Figures 3-4) and sea-ice volume. From the resulting sea-ice volume budget, we finally estimated the freshwater equivalents of local annual sea-ice-ocean fluxes due to freezing and melting and annual lateral sea-ice transport (Methods).

Uncertainties in these derived freshwater flux products are substantial (Methods). A major challenge arises from the need to combine sea-ice drift estimates from different satellites in order to estimate trends. We addressed potential inhomogeneities and biases by vigorous data quality control, several corrections, and considering different time periods (Methods). A second challenge is associated with the relatively limited number of observations of sea-ice thickness. These uncertainties plus the observationally constrained range of the other input quantities entered our error estimates of the final freshwater flux product (Extended Data Tables 1-2). In the Atlantic sector, uncertainties associated with the mean sea-ice thickness distribution dominate the uncertainty, while in the Pacific sector, uncertainties are mostly caused by uncertainties in sea-ice drift.

Our analysis reveals large trends in the meridional sea-ice freshwater transport in the Southern

Ocean between 1982 and 2008 (Figures 1b and 2c) affecting the regional sea-ice-ocean freshwater fluxes (Figure 2d). The annual northward sea-ice freshwater transport of 130±30 mSv (1 milli-Sverdrup = 10^3 m^3 s^{-1} ≈ 31.6 Gt yr^{-1}; Figure 2a; Extended Data Table 1) from the coastal to the open ocean region strengthened by +9±5 mSv per decade (Extended Data Table 2). Here, the coastal ocean refers to the region between the Antarctic coast and the zero sea-ice-ocean freshwater flux line, and the open ocean is the region between the zero sea-ice-ocean freshwater flux line and the sea-ice edge (Figure 2b). The increased northward transport caused, on average, an additional extraction of freshwater from the coastal ocean of −40±20 mm yr^{-1} per decade and an increased addition to the open ocean region of +20±10 mm yr^{-1} per decade.

The overall intensification occurred primarily in the Pacific sector where we find a vigorous northward freshwater transport trend of +14±5 mSv per decade. The trends in this sector are the most robust ones (Extended Data Table 3). Over the whole period, this change in the Pacific sector corresponds to an increase of about 30% with respect to the climatological mean in the entire Southern Ocean (Extended Data Table 1). Largest trends occurred locally in the high-latitude Ross Sea (Figure 2d), where our estimated trends agree well with a previous study[13] (Methods). The increase in the Pacific sector is partly compensated for by small decreases in the Atlantic and Indian Ocean sectors. We reach similar conclusions when we consider only the satellite data from 1992 through 2004, i.e., the period when they are least affected by potential inhomogeneities (Extended Data Table 3).

The reason for the observed northward sea-ice freshwater transport and its recent trends is the strong southerly winds over the Ross and Weddell Seas, which persistently blow cold air from Antarctica over the ocean, pushing sea ice northward[9]. The winds over the Ross Sea considerably strengthened in recent decades, possibly due to a combination of natural, multi-decadal variability, changes in greenhouse gases, and stratospheric ozone depletion[9]. These changes in southerly winds induced regional changes in northward sea-ice drift[8,9], which are responsible for the sea-ice freshwater transport trends (Methods). This relation between the atmospheric circulation and sea-ice drift changes enabled us to independently estimate the sea-ice drift anomalies using sea-surface pressure gradients along latitude bands from atmospheric reanalysis data[22] (Methods). Comparing the resulting northward sea-ice transport anomalies to the satellite-based estimates across the same latitude bands, results in a similar overall trend (Figure 3). Thus, this alternative approach not only corroborates our estimated long-term trend, but it also suggests that any remaining inhomogeneities in the sea-ice drift data due to changes in the satellite instruments are comparably small after applying multiple corrections (Methods).

To assess how the changing sea-ice-ocean freshwater flux (Figure 2d) affected the salinity in the Southern Ocean, we assumed that the additional freshwater in the open ocean region entered AAIW and SAMW formed from upwelling Circumpolar Deep Waters (CDW)[27,28] (Methods). We find that our freshwater flux trends imply a freshening at a rate of −0.02±0.01 g kg^{-1} per decade in the surface waters that are transported northward and form AAIW and SAMW (Figure 1b). Thus, the sea-ice freshwater flux trend could account for a substantial fraction of the observed long-term freshening in these water masses[1,3,4]. The strong sea-ice-ocean freshwater flux trends in the Pacific sector (Figure 2d) spatially coincide with the region of largest observed surface freshening[2,5] (Extended Data Figure 7) and can explain also the stronger freshening of the Pacific AAIW as compared to that of the Atlantic[1,4]. A more quantitative attribution of the observed salinity trends to the freshwater transport trends is beyond the scope of our study because the observed freshening trends stem from different time periods, and have strong regional variations and large uncertainties themselves[1,3,4]. However, our data show that changes in northward sea-ice freshwater transport induce salinity changes of comparable magnitude to the observed trends.

Our estimates in coastal regions (Figure 2d) also help to explain the observed salinity changes in AABW[6], which is sourced from this region. Additional glacial meltwater from West Antarctica[12] strongly freshened the continental shelf in the Ross and Amundsen Seas over recent decades[2,10,11] (Figure 1b). However, the observed freshening in Pacific and Indian Ocean AABW was found to be much smaller than expected by this additional glacial meltwater[6]. Our data suggests that the freshening induced by the increasing glacial meltwater is substantially reduced by a salinification from an increased sea-ice to ocean salt flux over the continental shelf in the Pacific sector. This salt flux trend corresponds to a freshwater equivalent of −10±3 mSv per decade, resulting from an increasing northward sea-ice export from this region of enhanced sea-ice formation (Figure 2c-d). In contrast, over the continental shelf in the Atlantic sector, our data suggests a decreasing sea-ice to ocean salt flux, corresponding to a freshwater equivalent of +6±3 mSv per decade, which may have contributed to the observed freshening of the newly formed Atlantic AABW[6] and the north-western continental shelf waters[18].

The large contribution of trends in sea-ice freshwater transport to recent salinity changes in the Southern Ocean is in line with the dominant role that sea ice plays for the surface freshwater budget in the seasonal sea-ice zone[29] and for the global overturning circulation[19–21,27] in the mean state. The freshwater equivalent of the total Southern Ocean sea-ice melting flux (Figure 4a) is as large as 460±100 mSv (Extended Data Table 1). On an annual basis, the vast majority of this melting flux is supported by the freezing of seawater of −410±110 mSv, with the remaining flux arising from snow-ice formation[30] (Methods; Figure 4b). Most of the sea ice is produced in the coastal region (−320±70 mSv), but only about 60% of the sea ice also melts there. The rest, i.e., 130±30 mSv is being exported to the open ocean (Figure 4c). These mean estimates agree well with an independent study carried out in parallel to this study[27], which is based on the assimilation of Southern Ocean salinity and temperature observations (Methods).

The process of northward freshwater transport by sea ice effectively removes freshwater from waters entering the lower oceanic overturning cell, in particular AABW, and adds it to the upper circulation cell, especially AAIW (Figure 1a). Hereby, the salinity difference between these two water masses and thus the meridional and vertical salinity gradients increase. In steady state, the northward sea-ice freshwater transport of 130±30 mSv implies a salinity modification of +0.15±0.06 g kg^{-1} and −0.33±0.09 g kg^{-1} in waters entering the lower and upper cell, respectively (Methods). The latter suggests that sea-ice freshwater transport accounts for the majority of the salinity difference between upwelling CDW and the exiting AAIW. We estimated that the salinification from sea ice in waters entering the lower circulation cell is compensated for by glacial meltwater and by an excess precipitation over evaporation in this region at about equal parts, agreeing with the very small salinity difference between CDW and AABW (Methods).

Because salinity dominates the density structure in polar oceans[14], our findings imply that sea-ice transport is a key factor for the vertical and meridional density gradients in the Southern Ocean and their recent changes (Figure 1). This interpretation is consistent with the observation that large areas of the upper Southern Ocean not only freshened but also stratified in recent decades[7]. Increased stratification potentially hampers the mixing of deeper, warmer, and carbon-rich waters into the surface layer and thus could increase the net uptake of CO_2[14,16,17]. Consequently, our results suggest that Antarctic sea-ice freshwater transport, through its influence on ocean stratification and the carbon cycle, is more important for changes in global climate[14,15] than has been appreciated previously. This implication of our findings for the climate system stresses the urge to better constrain spatial patterns as well as temporal variations of sea-ice-ocean fluxes by reducing uncertainties in observations of drift, thickness, and snow cover of Antarctic sea ice.

1. Wong, A. P. S., Bindoff, N. L. & Church, J. A. Large-scale freshening of intermediate waters in the Pacific and Indian oceans. *Nature* **400,** 440–443 (1999).
2. Jacobs, S. S., Giulivi, C. F. & Mele, P. A. Freshening of the Ross Sea during the late 20th century. *Science* **297,** 386–389 (2002).
3. Böning, C. W., Dispert, A., Visbeck, M., Rintoul, S. R. & Schwarzkopf, F. U. The response of the Antarctic Circumpolar Current to recent climate change. *Nat. Geosci.* **1,** 864–869 (2008).
4. Helm, K. P., Bindoff, N. L. & Church, J. A. Changes in the global hydrological-cycle inferred from ocean salinity. *Geophys. Res. Lett.* **37,** L18701 (2010).
5. Durack, P. J., Wijffels, S. E. & Matear, R. J. Ocean salinities reveal strong global water cycle intensification during 1950 to 2000. *Science* **336,** 455–458 (2012).
6. Purkey, S. G. & Johnson, G. C. Antarctic Bottom Water warming and freshening: contributions to sea level rise, ocean freshwater budgets, and global heat gain. *J. Clim.* **26,** 6105–6122 (2013).
7. de Lavergne, C., Palter, J. B., Galbraith, E. D., Bernardello, R. & Marinov, I. Cessation of deep convection in the open Southern Ocean under anthropogenic climate change. *Nat. Clim. Chang.* **4,** 278–282 (2014).
8. Holland, P. R. & Kwok, R. Wind-driven trends in Antarctic sea-ice drift. *Nat. Geosci.* **5,** 872–875 (2012).
9. Haumann, F. A., Notz, D. & Schmidt, H. Anthropogenic influence on recent circulation-driven Antarctic sea ice changes. *Geophys. Res. Lett.* **41,** 8429–8437 (2014).
10. Jacobs, S. S. & Giulivi, C. F. Large multidecadal salinity trends near the Pacific-Antarctic continental margin. *J. Clim.* **23,** 4508–4524 (2010).
11. Nakayama, Y., Timmermann, R., Rodehacke, C. B., Schröder, M. & Hellmer, H. H. Modeling the spreading of glacial meltwater from the Amundsen and Bellingshausen Seas. *Geophys. Res. Lett.* **41,** 7942–7949 (2014).
12. Paolo, F. S., Fricker, H. A. & Padman, L. Volume loss from Antarctic ice shelves is accelerating. *Science* **348,** 327–331 (2015).
13. Drucker, R., Martin, S. & Kwok, R. Sea ice production and export from coastal polynyas in the Weddell and Ross Seas. *Geophys. Res. Lett.* **38,** L17502 (2011).
14. Sigman, D. M., Hain, M. P. & Haug, G. H. The polar ocean and glacial cycles in atmospheric CO2 concentration. *Nature* **466,** 47–55 (2010).
15. Ferrari, R. *et al.* Antarctic sea ice control on ocean circulation in present and glacial climates. *Proc. Natl. Acad. Sci.* **111,** 8753–8758 (2014).
16. Frölicher, T. L. *et al.* Dominance of the Southern Ocean in anthropogenic carbon and heat uptake in CMIP5 models. *J. Clim.* **28,** 862–886 (2015).
17. Landschützer, P. *et al.* The reinvigoration of the Southern Ocean carbon sink. *Science* **349,** 1221–1224 (2015).
18. Hellmer, H. H., Huhn, O., Gomis, D. & Timmermann, R. On the freshening of the northwestern Weddell Sea continental shelf. *Ocean Sci.* **7,** 305–316 (2011).
19. Saenko, O. A., Schmittner, A. & Weaver, A. J. On the role of wind-driven sea ice motion on ocean ventilation. *J. Phys. Oceanogr.* **32,** 3376–3395 (2002).
20. Komuro, Y. & Hasumi, H. Effects of surface freshwater flux induced by sea ice transport on the global thermohaline circulation. *J. Geophys. Res.* **108,** 3047 (2003).
21. Kirkman, C. H. & Bitz, C. M. The effect of the sea ice freshwater flux on Southern Ocean temperatures in CCSM3: deep-ocean warming and delayed surface warming. *J. Clim.* **24,** 2224–2237 (2011).
22. Dee, D. P. *et al.* The ERA-Interim reanalysis: configuration and performance of the data assimilation system. *Q. J. R. Meteorol. Soc.* **137,** 553–597 (2011).
23. Meier, W. *et al.* NOAA/NSIDC Climate Data Record of passive microwave sea ice

concentration, version 2. 1980-2009. *Boulder, Colorado USA: National Snow and Ice Data Center* (2013). doi:10.7265/N55M63M1
24. Kurtz, N. T. & Markus, T. Satellite observations of Antarctic sea ice thickness and volume. *J. Geophys. Res. Ocean.* **117,** C08025 (2012).
25. Massonnet, F. *et al.* A model reconstruction of the Antarctic sea ice thickness and volume changes over 1980-2008 using data assimilation. *Ocean Model.* **64,** 67–75 (2013).
26. Fowler, C., Emery, W. J. & Tschudi, M. A. Polar Pathfinder daily 25 km EASE-Grid sea ice motion vectors, version 2. 1980-2009. *Boulder, Colorado USA: National Snow and Ice Data Center. Digital media, distributed in netCDF format by the Integrated Climate Data Center, University of Hamburg, Hamburg.* (2013).
27. Abernathey, R. P. *et al.* Water-mass transformation by sea ice in the upper branch of the Southern Ocean overturning. *Nat. Geosci.* Available online (2016). doi:10.1038/ngeo2749
28. Talley, L. D. Closure of the global overturning circulation through the Indian, Pacific, and Southern Oceans: Schematics and transports. *Oceanography* **26,** 80–97 (2013).
29. Tamura, T., Ohshima, K. I., Nihashi, S. & Hasumi, H. Estimation of surface heat/salt fluxes associated with sea ice growth/melt in the Southern Ocean. *SOLA* **7,** 17–20 (2011).
30. Massom, R. A. *et al.* Snow on Antarctic sea ice. *Rev. Geophys.* **39,** 413–445 (2001).

Acknowledgments. This work was supported by ETH Research Grant CH2-01 11-1 and by European Union (EU) grant 264879 (CARBOCHANGE). I.F. was supported by C2SM at ETH Zürich and the Swiss National Science Foundation Grant P2EZP2-152133. S.K. was supported by the Center of Excellence for Climate System Analysis and Prediction (CliSAP), University of Hamburg, Germany. F.A.H. and S.K. acknowledge the support from the International Space Science Institute (ISSI), Bern, Switzerland, under project #245. We are thankful to F. Massonnet for providing the sea-ice thickness reconstruction and discussion. The ICESat-1 sea-ice thickness data were provided by the NASA Goddard Space Flight Center. The ship-based sea-ice thickness data were provided by the SCAR Antarctic Sea Ice Processes and Climate (ASPeCt) program. We appreciate the provision of sea-ice concentration and motion data by the National Snow and Ice Data Center, the Integrated Climate Data Center at the University of Hamburg, and R. Kwok. We thank T. Frölicher, S. Yang, A. Stössel, M. Frischknecht, L. Papritz, P. Durack, M. van den Broecke, J. Lenaerts, and J. van Angelen, M. Meredith, as well as four anonymous reviewers for discussion, comments, and ideas.

Author contributions. F.A.H., M.M., and I.F. conceived the study. F.A.H. assembled the data and performed the analyses. F.A.H. and N. G. wrote the manuscript. M.M., I.F., and S.K. assisted during the writing process. S.K. assisted in the quality and uncertainty assessment. All authors developed the methods and interpreted the results. N.G. and M.M. supervised this study.

Data deposition. Sea-ice freshwater fluxes leading to the main conclusions are publicly available (http://dx.doi.org/10.16904/8). Other presented data is available from the corresponding author upon request.

Code availability. Climate Data Operators (CDO; version 1.6.8) used for part of the analysis are publicly available (http://www.mpimet.mpg.de/cdo). Other analytical scripts are available upon request from the corresponding author.

Competing financial interests. The authors declare no competing financial interests.

Corresponding author. Correspondence and requests for materials should be addressed to F. Alexander Haumann (alexander.haumann@usys.ethz.ch).

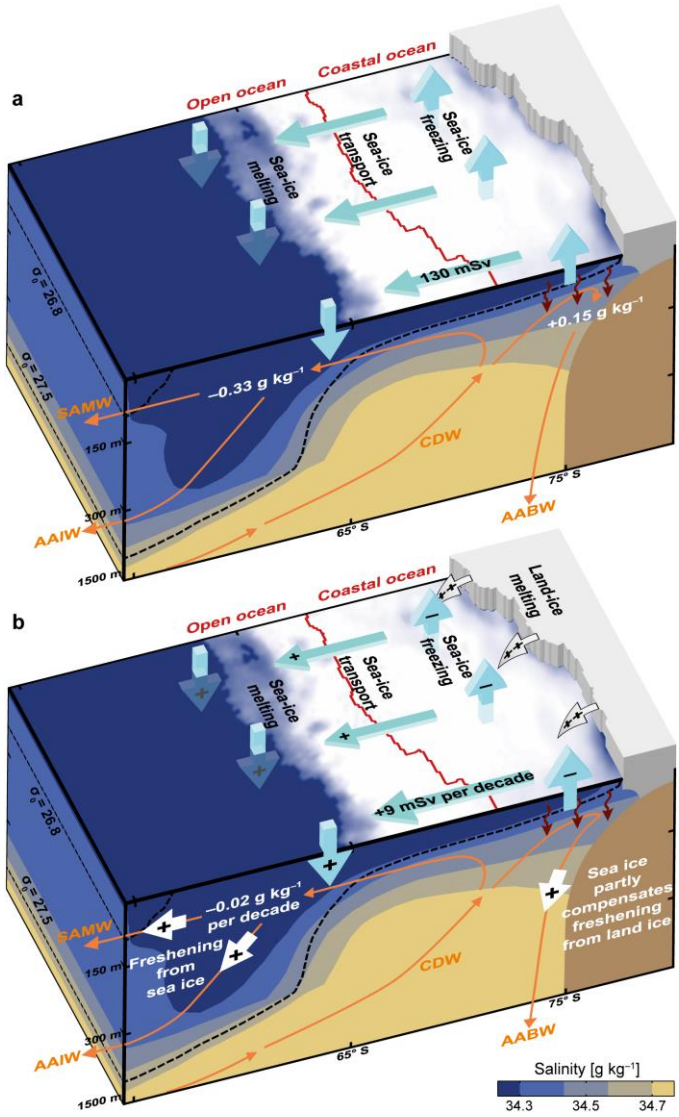

Figure 1 | Effect of northward sea-ice freshwater transport on Southern Ocean salinity. Schematic cross-section illustrating the effect of northward sea-ice freshwater transport (blue arrows) on (**a**) mean ocean salinity and (**b**) on the trends over the period 1982 through 2008 (Methods). The red line separates the open and coastal ocean regions. The increasing sea-ice transport freshened the open ocean and, by leaving the salt behind in the coastal region (red curved arrows), compensated for part of the freshening by enhanced glacial meltwater input (grey arrows). White arrows indicate the freshening effect from both sea ice and land ice. Positive fluxes are defined downward or northward. The background shows mean salinity (in colour) and density (dashed black lines) separating Circumpolar Deep Water (CDW) from Antarctic Intermediate Water (AAIW) and Subantarctic Mode Water (SAMW). Orange arrows: ocean circulation; AABW: Antarctic Bottom Water.

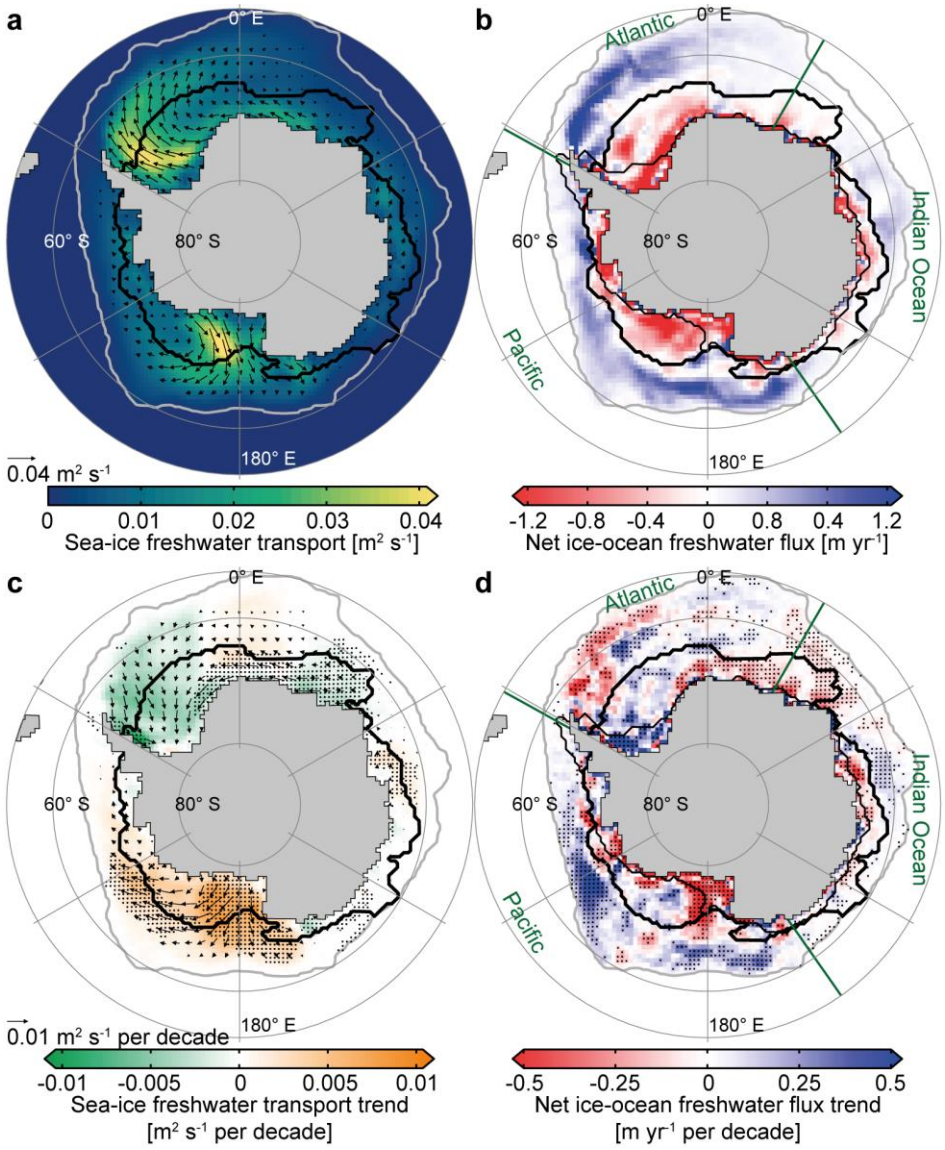

Figure 2 | Mean state and trends of net annual freshwater fluxes associated with sea ice over the period 1982 through 2008. a, Mean sea ice induced freshwater transport. **b,** Mean net sea-ice-ocean freshwater flux. **c, d,** Linear trends of northward sea-ice freshwater transport (c) and net sea-ice-ocean freshwater flux from freezing and melting (d). Stippled trends are significant at the 90% level (Methods). Arrows: (a) mean and (c) trend of the annual transport vectors; thick black lines: zero sea-ice-ocean freshwater flux line dividing the coastal from the open ocean regions; thin black lines: continental shelf (1000-m isobath); grey lines: sea-ice edge (1% sea-ice concentration); green lines: basin boundaries.

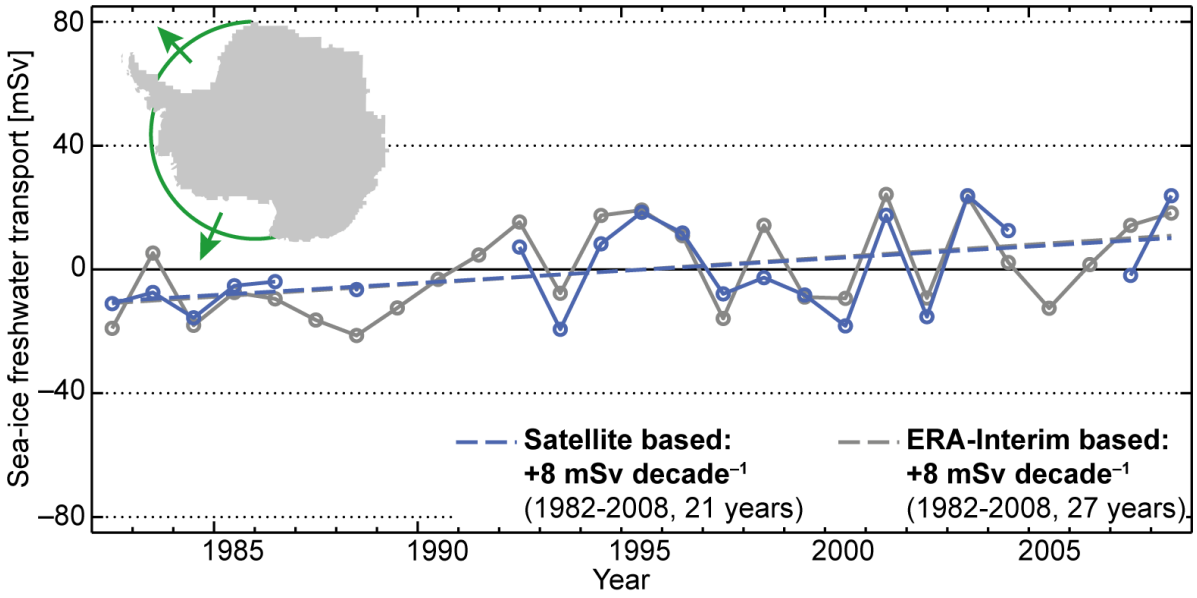

296

297 **Figure 3 | Time series of annual northward sea-ice freshwater transport anomalies across**
298 **latitude bands.** The underlying sea-ice drift data are based on two independent data sources,
299 i.e., the corrected NSIDC satellite data (blue; only consistent years) and zonal sea-level pressure
300 gradients from ERA-Interim data (grey; Methods). Dashed lines show the respective linear
301 regressions. Inserted map shows the latitude bands in the Atlantic (69.5° S) and Pacific (71° S)
302 sectors.

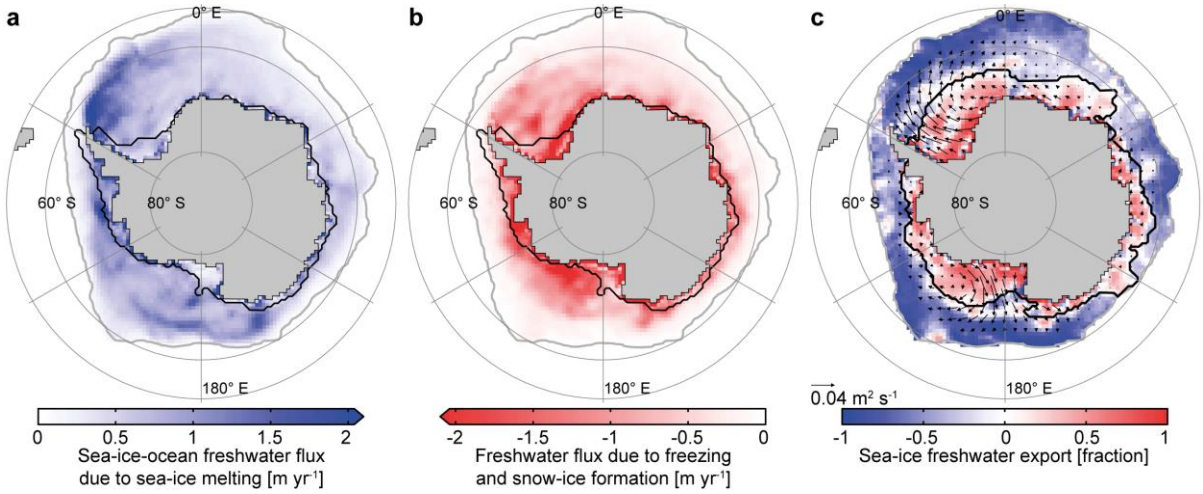

303

304 **Figure 4 | Mean annual sea-ice related freshwater fluxes associated with melting, freezing,**
305 **and transport over the period 1982 through 2008. a,** Sea-ice-ocean freshwater flux due to
306 melting. **b,** Freshwater flux associated with freezing and snow-ice formation. **c,** Fraction of
307 freshwater exported relative to local freezing flux (red) and imported relative to the local
308 melting flux (blue) due to sea-ice induced freshwater transport (arrows). Black and grey lines
309 as in Figure 2.

310

Methods

Data. Satellite-derived sea-ice concentration stems from the Climate Data Record (CDR; version 2; 1980 to 2009; http://dx.doi.org/10.7265/N55M63M1)[23] that comprises data from the NASA Team algorithm (NTA)[31] and the Bootstrap algorithm (BA; version 2)[32], as well as a merged data set. Sea-ice thickness data stems from a reconstruction with the ocean-sea-ice model NEMO-LIM2 (1980 to 2009)[25], from the laser altimeter ICESat-1 (2003 to 2008; http://seaice.gsfc.nasa.gov)[24], as well as from ship-based observations (ASPeCt; 1980 to 2005; http://aspect.antarctica.gov.au)[33]. Satellite-derived sea-ice drift stems from the National Snow and Ice Data Center (NSIDC, version 2; 1980 to 2009, http://nsidc.org/data/nsidc-0116)[26] and is corrected by drifting buoy data (1989 to 2005)[34]. We used an alternative sea-ice drift product for the uncertainty estimation (Kwok et al.; 1992 to 2003; http://rkwok.jpl.nasa.gov)[35,36]. Additionally, we used daily atmospheric sea-level pressure, surface air temperature, and 10-m wind speed from the ERA-Interim reanalysis (1980 to 2009, http://apps.ecmwf.int)[22]. We provide a detailed description of the data processing in the corresponding sections below.

Sea-ice concentration. We used all three sea-ice concentration products available from the CDR[23] (data section). If any of the grid points in either the merged, NTA, or BA product shows 0% sea-ice concentration, all products are set to 0% sea-ice concentration. We used a first order conservative remapping method from the Climate Data Operators (CDO, version 1.6.8)[37] to interpolate the sea-ice concentration to the sea-ice drift grid. The BA performs superior compared to the NTA around Antarctica as the NTA underestimates sea-ice concentrations by 10% or more[23,38] (Extended Data Figures 1a-b). Therefore, we primarily used the BA product. However, BA potentially underestimates sea-ice concentration in presence of thin sea ice and leads[23,38]. Therefore, we used the merged product that should be more accurate in these regions[23] to estimate the uncertainties. Generally, sea-ice concentration is the best constrained of the three sea-ice variables. Its contribution to the climatological mean flux uncertainty is below 1% (Extended Data Table 1). To obtain the uncertainty in the freshwater flux trends, we additionally used the NTA because differences in the Antarctic sea-ice area trends between the BA and NTA have been reported[39]. Differences between the BA and NTA sea-ice concentration trends range from 10% to 20% relative to the actual trend (Extended Data Figures 1c-d). The associated uncertainties in the spatially integrated sea-ice freshwater flux trends are about 10% (Extended Data Table 2).

Sea-ice thickness. Sea-ice thickness data spanning our entire analysis period do not exist, mostly owing to challenges in remote sensing of Antarctic sea-ice thickness[40]. Therefore, we used a sea-ice thickness reconstruction[25] (data section) from a model that assimilated the observed sea-ice concentration. Through the assimilation, the model constrained air-sea heat fluxes, improving the spatial and temporal variability of sea-ice thickness. The model did not assimilate sea-ice thickness observations themselves. Sea-ice thickness, as we use it here, is not weighted with sea-ice concentration and does not include the snow layer.

The reconstruction overestimates the sea-ice thickness in the central Weddell and Ross Seas and underestimates it in some coastal regions compared to the ICESat-1[24] and ASPeCt[33] data sets (data section; Extended Data Figure 2). To compare the different sea-ice thickness data sets, we interpolated the reconstruction, ICESat-1, and ASPeCt data to the sea-ice drift grid using CDO[37] distance-weighted averaging. For our best estimate of the sea-ice freshwater fluxes, we applied a weighted bias correction to the reconstruction using the spatially gridded version of the ICESat-1 data (see below). Both the ICESat-1 and ASPeCt data sets are potentially biased low, particularly in areas with thick or deformed sea ice[33,40–42], where we found the largest differences between these two data sets and the uncorrected reconstruction.

Thus, the thicker sea ice in the Weddell Sea in the uncorrected reconstruction might yet be realistic, especially when considering alternative ICESat-1 derived estimates for this region[40,43,44]. To capture the full uncertainty range associated with the mean sea-ice thickness distribution, we used the difference between the uncorrected reconstruction and the ICESat-1 data. Uncertainties in sea-ice thickness dominate the climatological freshwater flux uncertainties in the Atlantic and Indian Ocean sectors, ranging from 10% to 35%, and are also substantial in all other regions and for the overall trends (Extended Data Tables 1-2).

For the correction of the mean sea-ice thickness distribution, we first calculated relative differences to ICESat-1 whenever data were available. Then, we averaged all differences that were within two standard deviations over time. We applied this average, relative bias correction map to the data at each time step. To ensure that local extremes were not exaggerated, we used weights. Weights were one for a sea-ice thickness of 1.2 m, i.e., the full bias correction was applied, and decreased to zero for sea-ice thicknesses of 0.2 m and 2.2 m, i.e., no bias correction was applied. We derived these thresholds empirically to reduce biases with respect to the non-gridded ICESat-1 and ASPeCt data (Extended Data Figure 2). Trends in the reconstruction remain largely unaffected by the bias correction (comparing Extended Data Figure 2a and the original trend[25]).

Local extremes in the sea-ice thickness reconstruction, caused by ridging events, are most likely inconsistent with the observed sea-ice drift and would lead to unrealistic short-term variations in our final fluxes. However, when considering net annual melting and freezing fluxes and averages over large areas these variations cancel. To reduce the noise in our data set, we filtered extremes with a daily sea-ice thickness anomaly larger than 2 m with respect to the climatological seasonal cycle, representing only 0.1% of all data points. These and other missing grid points (in total 2.6%) were interpolated by averaging the neighbouring grid points. We also calculated our sea-ice freshwater fluxes based on the unfiltered data and included these fluxes in our uncertainty estimate.

Snow-ice formation due to flooding and refreezing[30,45] is part of the estimated sea-ice thickness. As snow-ice forms partly from the atmospheric freshwater flux and not from the ocean alone, it could lead to an overestimation of the total ocean to sea-ice freshwater flux due to freezing. The amount of snow-ice formation is highly uncertain[30,45] but within the uncertainty of the sea-ice thickness. To account for this process, we reduced the freezing fluxes according to snow-ice formation estimates from the reviewed literature[30]. In the Atlantic, Indian Ocean, and Pacific sectors, we applied approximate snow-ice formation rates of 8±8%, 15±15%, and 12±12% of the freezing flux, respectively[30]. In the entire Southern Ocean, the amount of snow that is transformed to ice would thus amount to about 50 mSv, or about 35% of the suggested atmospheric freshwater flux onto Antarctic sea ice[27].

Trends in sea-ice thickness (Extended Data Figure 2a) are highly uncertain but broadly agree among different modelling studies[25,46,47]. To show that our results are robust with respect to the less certain trends or short-term variations in sea-ice thickness, we compared our estimated transport trends across the latitude bands (3) with a sensitivity analysis, where we kept the sea-ice thickness constant. The resulting transport trends across the latitude bands of about −6 mSv per decade in the Atlantic sector and about +11 mSv per decade in the Pacific sector are still within our estimated uncertainty (Extended Data Table 2). Most of the sea-ice thickness trends (Extended Data Figure 2a) occur either north (Pacific sector) or south (Atlantic sector) of the zero freshwater flux line or latitude bands. Thus, the trend in sea-ice thickness does not considerably affect the northward sea-ice freshwater transport trend. However, the mean sea-

ice thickness uncertainty at the zero freshwater flux line is the largest contributor to the overall northward sea-ice freshwater transport trend (Extended Data Table 2).

Sea-ice drift. We used the gridded version of the NSIDC[26] (data section) sea-ice drift data set. In the Antarctic, it is based on five passive microwave sensors[48,49] and the Advanced Very High Resolution Radiometer (AVHRR)[50] data (Extended Data Figure 4). Two studies validated this data set with buoy data in the Weddell Sea (1989 through 2005)[34] and around East Antarctica (1985 to 1997)[51]. There is a very high correlation between the buoy and the satellite data on large temporal and spatial scales (i.e., monthly and regional) and a strongly reduced agreement on smaller scales (i.e., daily and local)[34,51]. The satellite-derived sea-ice drift underestimates the sea-ice velocity given by the buoys by 34.5%[34], i.e., faster drift velocities have a larger bias[52]. The bias is smaller for the meridional (26.3%) than for the zonal drift[34]. We here corrected for these low biases by multiplying the drift velocity with the correction factor (1.357) that corresponds to the meridional drift bias[34]. We argue that the meridional component of the bias is the better estimate in the central sea-ice region, which is the key region for our results. Here, the drift is mainly meridional. The larger biases are observed in the swift, mostly zonal drift along the sea-ice edge causing the larger zonal biases. The spatial dependence of the bias and our correction imply that larger biases and uncertainties remain in our final product around the sea-ice edge.

We further processed this bias-corrected drift data. First, we removed all data flagged as bad in the product. Second, we removed any data with sea-ice concentrations below 50%, closer than 75 km to the coast[34], or with a spurious, exact value of zero. Our results are not sensitive to this filtering but it reduces the spatial and temporal noise. After these modifications, about 75% of all grid cells covered by sea ice had an associated drift vector.

We compared both the original and the bias-corrected data to a partly independent product by Kwok et al.[35,36] (data section). We interpolated these data onto our grid using CDO[37] distance weighted averaging and applied the same 21-day running mean as for the NSIDC sea-ice drift data. We compared sea-ice drift vectors whenever both data sets were available and sea-ice concentrations were larger than 50%. Extended Data Figure 3 shows the meridional drift components prior (a) and after applying the bias correction factor from the buoy data (b). We find that the agreement between the two data sets is much higher after the corrections. Compared to the original NSIDC sea-ice drift data set, the largest improvement occurs in the slope: 1.06 compared to 1.55. Root-mean-square differences and the linear correlation coefficient remain identical and the absolute bias is reduced by 0.2 km/day. Correlation coefficients between the two data sets are 0.8 for both the zonal and meridional drift component. The spatial patterns of the mean annual sea-ice drift speed (Extended Data Figure 3c-e) illustrate the improvement in agreement between the two data sets after the application of the bias correction but confirm that considerable differences remain at the sea-ice edge. These differences lead to a relatively high root-mean-square difference of the annual mean sea-ice drift speed in these regions (Extended Data Figure 3f). However, in the central sea-ice pack–the region that is crucial for our results–the root-mean-square differences are much smaller.

Our bias-corrected sea-ice drift speeds are typically slightly lower (about 9% to 19%) than those by Kwok et al. but considerably higher than in the uncorrected NSIDC data (about 26%, see above). We used these differences between the data sets to estimate the uncertainties induced by sea-ice drift on the final product (Δu in Extended Data Tables 1-2): First, we re-computed all fluxes by correcting the original NSIDC data with correction factors derived from the Kwok et al. data (1.82 or 45% for the zonal drift, and 1.55 or 35% for the meridional drift) instead of the buoy-derived correction factor. This way, we also accounted for an uncertainty in the drift

direction. Then, we averaged the deviations between our best estimate and the Kwok et al. based estimate with those between our best estimate and using the uncorrected and unfiltered NSIDC data. Uncertainties from sea-ice drift in the freshwater fluxes are about 20%. They considerably contribute to the final freshwater flux uncertainty and our trend uncertainties in all regions.

Sea-ice-ocean freshwater flux. We estimated annual net sea-ice-ocean freshwater fluxes over the period 1982 through 2008 by calculating the local sea-ice volume change and divergence[8,53]. From this, we derived, through a mass balance, the local freshwater fluxes F ($m^3\ s^{-1}$) from the sea ice to the ocean due to freezing and melting on a daily basis:

$$F = -C_{fw}\left(\frac{\partial(A\ c\ h)}{\partial t} + \nabla\cdot(A\ c\ h\ \vec{\boldsymbol{u}})\right). \quad (1)$$

The four variables c, h, $\vec{\boldsymbol{u}}$, and A denote the sea-ice concentration, thickness, drift velocity, and grid-cell area, respectively. The factor C_{fw} converts the sea-ice volume flux to a freshwater equivalent[54]:

$$C_{fw} = \frac{\rho_{ice}(1 - s_{ice}/s_{sw})}{\rho_{fw}}. \quad (2)$$

Here, ρ_{ice}, s_{ice}, s_{sw}, and ρ_{fw} are sea-ice density (925 kg m^{-3})[55], sea-ice salinity (6 g kg^{-1})[56], reference seawater salinity (34.7 g kg^{-1})[28], and freshwater density (1000 kg m^{-3}), respectively.

Annual sea-ice freshwater fluxes were computed from the daily fluxes from March to February of the next year (i.e., March 1982 to February 2009), which corresponds to the annual freezing and melting cycle of sea ice in the Southern Ocean[53]. Remaining imbalances between, e.g., the open and coastal ocean of the Atlantic sector (Extended Data Tables 1-2) are due to multiyear sea ice in the coastal region. We performed all calculations on the grid of the sea-ice drift data[26] and averaged all data products over three by three grid boxes resulting in a nominal resolution of 75 km. To obtain the zero freshwater flux contour line, we averaged the climatological fluxes over nine by nine grid boxes. To estimate melting and freezing fluxes, we separately summed up positive and negative daily fluxes over a year (Figures 4a-b). As temporal fluctuations accumulate when only adding positive or negative values, noise can lead to an overestimation of these fluxes. Therefore, each of the sea-ice variables (c, h, and $\vec{\boldsymbol{u}}$) were low-pass filtered using a 21-day running mean.

Sea-ice freshwater transport. The total northward sea-ice volume transport ($m^3\ s^{-1}$) between the coastal and open ocean region equals the spatial integral of the divergence term in (1) in either of the two regions (Gauss's Theorem). We chose the open ocean region since there is considerable zonal exchange between the Indian Ocean and Atlantic sectors (Figure 2a) in the coastal region, influencing the sector based estimates. In the open ocean, this effect is negligible. We used this approach for the reported transport estimates (Extended Data Tables 1-3 and Extended Data Figures 5a-c).

To demonstrate that our main findings are robust on a basin-scale, and not influenced by small scale noise and local uncertainties, we also calculated the northward sea-ice freshwater transport across the latitude bands 69.5° S in the Atlantic sector and 71° S in the Pacific sector (Figure 3). To this end, we averaged sea-ice concentration, thickness, and meridional drift (c_n,

h_n, and v_n) in 1° longitude segments (n) along these latitudes and calculated the local freshwater transport T_n ($m^3\ s^{-1}$):

$$T_n = C_{fw}\ c_n\ h_n\ v_n\ \Delta l_n. \quad (3)$$

Here Δl_n denotes the length of the latitude increment n along the boundary and C_{fw} is defined in (2). Both sectors together show an annual northward freshwater transport of 100±30 mSv with an increase of 8±5 mSv per decade over the period 1982 to 2008 (Extended Data Figure 5d and Figure 3). This compares well with the mean (120±30 mSv) and trend (9±5 mSv per decade) of our spatially integrated sea-ice-ocean fluxes in the Pacific and Atlantic (Extended Data Figures 5b-c).

We calculated the spatial pattern of the sea-ice freshwater transport $\vec{\boldsymbol{f}}$ ($m^2\ s^{-1}$) as displayed in Figures 2a and c through:

$$\vec{\boldsymbol{f}} = C_{fw}\ c\ h\ \vec{\boldsymbol{u}}. \quad (4)$$

Time-series homogenisation. Our analysis and earlier studies[9,57] revealed major temporal inhomogeneities in the NSIDC sea-ice drift data set at the transitions between satellite sensors (Extended Data Figure 4). We argue that these temporal inhomogeneities are linked to the unavailability of the 85/91 GHz channels and sparser data coverage in the earlier years. The drift speed before 1982 appears underestimated, which is to some extent mitigated by AVHRR data thereafter. From 1982 to 1986, the drift speed is consistent but has a low bias. The drift ramps up in 1987, when the 85 GHz channels became available, and decreases again between 1989 and 1991, when these channels degraded[58]. A final sudden decrease occurs from 2005 to 2006 when 85 GHz data were not used. We used wind speed data over the sea ice from ERA-Interim[22] (data section) as an independent data source and scaled it to the sea-ice drift velocity for comparison (Extended Data Figures 4b). The scaling factor stems from the consistent years in the period 1988 to 2008 and varies in space and with season[59,60]. This analysis supports our argument that the sea-ice drift speed is underestimated when the higher resolution 85/91 GHz channels were not available. We note that the meridional drift seems less sensitive to these inhomogeneities than the total drift, which might be related to a higher data availability in the central sea-ice pack and is consistent with the lower biases found in the meridional sea-ice drift.

The spurious increase of the sea-ice velocity would affect our estimated trends if they were not taken into account (Extended Data Figures 5-6). Thus, we corrected the annual divergence (1) and lateral transport (3-4) for the sensor-related temporal inconsistencies as follows: We excluded the inconsistent years 1980 and 1981, 1987, 1989 to 1991, 2005, and 2006 from the analysis. To homogenise the years 1982 to 1986 with the years 1988 to 2008, i.e., remove the spurious trend in 1987, we first calculated linear regression lines prior and after 1987 at each grid point. Then, we added the differences between the end (1986) and start (1988) points of the regression lines to all years prior to 1987, i.e., assuming a zero change in the year 1987. Fitting regressions prior and past spurious jumps is a common procedure to homogenise climate data[61,62]. Here, we used a linear regression that serves the purpose of computing long-term trends in the time series.

To estimate the sensitivity of the trends in northwards sea-ice freshwater transport to uncertainties associated with the offset correction before 1987 (orange and green, Extended Data Figure 5), we performed a Monte Carlo analysis by varying the offset and estimating the resulting trends. We generated 10^4 normally distributed offsets around our best guess (about 19±5 mSv for the entire Southern Ocean; Extended Data Table 3). The standard deviation of this distribution was chosen to match the offset uncertainty that arises from the root-mean-square errors of the trends in each of the two time intervals 1982 to 1986 and 1988 to 2008. For each of these generated offsets, we then estimated the trends and their significance (Extended Data Table 3). For both the entire Southern Ocean and the Pacific sector, all sampled offsets yield a positive northward sea-ice freshwater transport trend. All trends for the Pacific sector and 92% for the entire Southern Ocean are positive and at the same time significant. Thus, our trend results are insensitive to uncertainties in the applied homogenization at the 90% confidence level. The posterior uncertainty shows that the uncertainty associated with the offset has no noticeable effect on the total uncertainty range, i.e., is smaller than ±1 mSv per decade.

Uncertainty estimation. Uncertainties of local (grid-point based) fluxes and time scales shorter than one year are probably large, due to potential inconsistencies between the data sets on such scales and an amplification of the uncertainties by the spatial and temporal differentiations in (1). Integrating these terms in space and time greatly reduces these uncertainties (Extended Data Tables 1-2). We estimated uncertainties in our product that are associated with the underlying input variables c, h, and $\vec{\boldsymbol{u}}$ by using their observationally constrained range from different data sources, including the applied corrections and filtering as described in the corresponding sections. Additionally, we used an averaging period of 31 days, instead of 21 days, and, for trends only, an estimate without a running-mean filter, to obtain uncertainty estimates associated with temporal noise (Δt). The results confirmed that only the annual melting or freezing fluxes, but not the net annual fluxes, are sensitive to the low-pass filtering as in the latter product the noise is averaged out. The sensitivity of the spatially integrated values to variations of the zero freshwater flux line is estimated by varying the smoothing radius from two to six grid boxes (ΔA). The uncertainty associated with the constant conversion factor (ΔC_{fw}; equation 2) is about 5% when using a realistic range of values[28,55,56]. For the trends only, we computed the standard error of the slope from the variance of the residuals around the regression line (Δs_e)[63]. The total uncertainty for both the climatological mean and the trends was estimated by calculating the root-mean-square of the individual contributions. This analysis shows that in the Atlantic and Indian Ocean sectors both the uncertainties in the climatology and trends (Extended Data Tables 1-2) are dominated by uncertainties in the sea-ice thickness. In contrast, the uncertainty in sea-ice drift dominates the uncertainty in the Pacific sector. We tested the significance of the trends with a t-test, accounting for the fact that only 21 out of 27 years were used and for a lag-one autocorrelation[63]. To indicate the significance of the trends at grid-point level (Figures 2c-d and Extended Data Figure 6), at which the data uncertainties are unknown, the local root-mean-square of the variance of the residuals was artificially increased by 40%, approximately corresponding to our data uncertainty estimate in Extended Data Table 2. The quality of our data directly at the coastline and around the sea-ice edge is reduced due to the limited quality and quantity of the underlying observations in these regions.

Sea-ice freshwater flux evaluation. A modelling study[27], carried out in parallel to this study, calculated freshwater fluxes associated with sea-ice formation, melting, and transport in the Southern Ocean State Estimate (SOSE). This model assimilates a large amount of observational data and optimizes surface fluxes. They estimated an annual sea-ice-ocean freshwater flux due to sea-ice formation of −360 mSv over the entire Southern Ocean, which is within our estimated range of −410±110 mSv. Moreover, they estimated that the combined annual sea-ice-ocean freshwater flux due to sea-ice and snow melting is about 500 mSv. Thus, in their estimate a

total of 140 mSv of snow accumulated on the sea ice. Our estimates partly include snow accumulation on sea ice, because part of the sea-ice thickness results from snow-ice formation, which we estimated to be about −50 mSv (section on sea-ice thickness). However, the snow layer on top of the sea ice is not included in our estimate of the freshwater flux due to sea-ice melting of 460±100 mSv. In that study[27], the authors estimate that the lateral sea-ice freshwater transport from the density class of CDW to AAIW and SAMW amounts to 200 mSv in the period between 2005 and 2010. Their estimate slightly differs from our estimated transport from the coastal to the open ocean that ranges between about 140 mSv and 160 mSv in 2007 and 2008 (Extended Data Figure 5). The reasons might be the slightly different regions and that their estimate also includes the transport of the snow layer on top of the sea ice.

Given the reduced confidence in the local fluxes (e.g. sea-ice production in coastal polynyas), it is reassuring that our data agree within our estimated range of uncertainty with previous estimates of mean fluxes for some larger coastal polynya regions[64,65]. Our confidence is higher for fluxes integrated over larger regions such as the high-latitude Ross and Weddell Seas (Extended Data Figure 5e). Here our estimates are in close agreement with previous studies as discussed in the following.

In the Ross Sea, we estimated that the northward transport from the coastal region across a flux gate between Land Bay and Cape Adare[36] (turquoise area in Extended Data Figure 5e) is 23±5 mSv, increasing by about 30% (or +7±4 mSv) per decade in the period 1992 to 2008. Based on the same passive microwave data but using a different algorithm for retrieving the sea-ice motion data, two studies[36,66] found a mean sea-ice area flux across this flux gate of about 10^6 km^2 between March and November in the periods 1992 to 2003[36] and 1992 and 2008[66], respectively. Using an approximated mean sea-ice thickness (0.6 m)[13,66] and the conversion factor (2), this corresponds to a mean northward freshwater transport of about 19 mSv. In close agreement with our estimate, these studies found an increase of 30% per decade (about +6 mSv per decade). Another study[13], using sea-ice motion from the Advanced Microwave Scanning Radiometer-EOS (AMSR-E), estimated that the mean sea-ice area flux between April and October (2003 to 2008) across the same flux gate is about 9.3×10^5 km^2 corresponding to a freshwater transport of about 23 mSv. Based on the same data but using an alternative approach[67], they found that the total sea-ice production in all Ross Sea polynyas together was about 737 km^3 between April and October (2003 to 2008), corresponding to a sea-ice-ocean freshwater flux of −31 mSv. This estimate is similar to the total production of about −36±7 mSv south of the flux gate in our data set, because most of the sea-ice production of this region occurs in the polynyas[13]. Using passive microwave data, the same study[13] found an increase of the production in the Ross Sea polynyas of 28% per decade between 1992 and 2008. A modelling study[68] found a net annual sea-ice-ocean freshwater flux due to melting and freezing of −27 mSv on the continental shelf in the Ross Sea, which is in agreement with our estimate of −23±5 mSv. They also found a long-term (unquantified, see their Figure 9b) decrease of the net annual sea-ice-ocean freshwater flux over the Ross Sea continental shelf in the period 1963 to 2000, which is qualitatively in line with our results.

In the Weddell Sea, the northward sea-ice area flux across a flux gate close to the 1000 m isobaths (blue area in Extended Data Figure 5e) has been found to be 5.2×10^5 km^2 based on AMSR-E data between April and October (2003 to 2008)[13]. Using an approximated mean sea-ice thickness (0.75 m)[13] and the conversion factor (2), this corresponds to a mean northward freshwater transport of about 16 mSv. This agrees well with our estimate of an annual northward transport of 16±4 mSv for the same years and the same region. Similar to the Ross Sea, the production in the major polynyas of the Weddell Sea was estimated[13]. However, in the Weddell Sea, a large fraction of the sea-ice transported across the flux gate is not produced in the coastal

polynyas[13], i.e., we cannot directly compare our large-scale estimate to the sea-ice production in the polynyas. In the same study[13], based on passive microwave data, they found a small, but insignificant long-term decrease of the sea-ice production in the Weddell Sea polynyas between 1992 and 2008, which is qualitatively consistent with our findings in the Atlantic sector. For a much larger area in the Weddell Sea, a modelling study[69] estimated an annual northward sea-ice freshwater transport of about 34 mSv and another observational study[70], mostly based on moorings and wind speed, estimated that this flux is as large as about 38±15 mSv. These estimates agree well with our finding of an annual northward freshwater transport of 41±18 mSv across the 69.5° S latitude band, which is approximately their considered transect.

Sea-ice freshwater transport based on ERA-Interim data. To support our findings, we quantified changes in sea-ice motion induced by changes geostrophic winds[59,60,70,71] from daily ERA-Interim[22] sea-level pressure and surface air temperature (data section). We averaged the data over 1° longitudinal segments along the previously defined latitude bands (Figure 3), computed 21-day running means, and smoothed the data spatially over 7 longitude bins. Then, we calculated the sea-level pressure gradients along the latitude bands and used these together with the atmospheric surface density to estimate geostrophic winds normal to the latitude bands[59,71]. From these, we calculated the sea-ice drift speed using a drift-to-wind-speed ratio of 0.016, derived from drifting buoys in the central Weddell Sea[59,71]. This parameter is strongly variable in space and time, which is a major uncertainty in the resulting sea-ice drift. Nevertheless, it provides an average estimate for the mostly free drifting sea ice in the central Antarctic sea-ice pack[59,71].

The resulting northward sea-ice freshwater transport (3) is independent in terms of the sea-ice drift but not in terms of the sea-ice concentration and thickness. We used anomalies (at each 1° increment) since the absolute values of the local transport are likely biased by local influences of ocean currents and sea-ice properties. The resulting total annual anomalies of the northward sea-ice freshwater transport agree well in terms of variability and long-term trend with the transport anomalies based on the satellite sea-ice drift (+8 mSv per decade; Figure 3). These estimates do not suffer from the temporal inhomogeneities that we identified in the satellite sea-ice drift data (section on time-series homogenisation).

Sea-ice contribution to ocean salinity. We determined the evolution of ocean salinity s (g kg^{-1}) in response to a given surface freshwater flux F (m^3 s^{-1}) from a combination of mass and salt balances. The mass balance for a given, well-mixed ocean surface box of volume V and density ρ reads:

$$\frac{d\rho V}{dt} = \rho_{in} Q_{in} + \rho_{fw} F - \rho Q_{out}, \tag{5}$$

where Q_{in} and Q_{out} (m^3 s^{-1}) are the volume fluxes of seawater in or out of the box, ρ_{in} (kg m^{-3}) is the respective density. In a steady state, the above equation (5) yields:

$$\rho_{in} Q_{in} = \rho Q_{out} - \rho_{fw} F. \tag{6}$$

The corresponding salt balance reads:

$$\rho V \frac{ds}{dt} = \rho_{in} Q_{in} s_{in} - \rho Q_{out} s, \tag{7}$$

We assumed the same constant source water salinity $s_{in} = s_{sw}$ and freshwater density ρ_{fw} as in (2), and used a constant reference density (ρ = 1027 kg m^{-3}). Moreover, we used the formation rate of the modified water mass as the volume flux of seawater out of the surface box ($Q_{out} = Q$). Then, substituting (6) in (7) yields:

$$\rho V \frac{ds}{dt} = (\rho Q - \rho_{fw} F) s_{sw} - \rho Q s. \quad (8)$$

In a steady state, this results in an equation that describes the modified salinity s:

$$\rho Q s = (\rho Q - \rho_{fw} F) s_{sw}. \quad (9)$$

Using $s = s_{sw} + \Delta s$, where Δs is the salinity difference between the source and modified water masses, (9) reduces to:

$$\Delta s = -\frac{\rho_{fw} s_{sw} F}{\rho Q}. \quad (10)$$

We used net water-mass transformation rates (Q) of 29 Sv between CDW and AABW and 13 Sv between CDW and AAIW/SAMW[28]. Figure 1a illustrates the results and shows the zonal mean ocean salinity and density distribution[72] for comparison.

Assuming that +130±30 mSv of freshwater enter CDW through northward sea-ice freshwater transport, the salinity modification (10) is −0.33±0.09 g kg^{-1}. The uncertainty includes a ±2 Sv uncertainty in the water-mass formation rate. In observations, the salinity difference between CDW and AAIW and SAMW ranges from about −0.3 to −0.5 g/kg[28]. Thus, northward freshwater transport by sea-ice could explain the majority of the salinity modification, consistent with very recent findings[27] and a mixed-layer salinity budget[73].

Similarly, we calculated the contribution of −130±30 mSv of freshwater removed from coastal regions due to northward sea-ice transport to the salinity modification (10) between CDW and AABW, obtaining an increase of +0.15±0.06 g kg^{-1}. The uncertainty includes a ±7 Sv uncertainty in AABW formation. However, observed salinity differences between the CDW and AABW are generally small or even of opposite sign[74]. This is the result of a compensating effect between a sea-ice driven salinification and a freshening from glacial and atmospheric freshwater. Freshwater fluxes from land ice through basal and iceberg melting are about +46±6 mSv and +42±5 mSv, respectively[75]. Assuming that roughly 60% of the icebergs melt in the coastal regions[76], a total of about +70 mSv are added from the land ice to the coastal ocean, corresponding to a freshening of about −0.08 g kg^{-1} or a compensation of the sea-ice freshwater flux of about 55% in AABW. We estimated from the ERA-Interim atmospheric reanalysis data[22] that the net atmospheric freshwater flux in the coastal region is about +80 mSv, corresponding to a freshening of about −0.09 g kg^{-1}. The resulting net salinity change in coastal waters from sea-ice, atmospheric, and land-ice freshwater fluxes is almost zero (−0.02 g kg^{-1}). Such a compensation of the freshwater fluxes in coastal regions was noticed previously[69,77]. We note that large regional variations of these fluxes have been reported[75,78].

To estimate the temporal salinity changes at the surface and in newly formed AAIW and SAMW, we assumed a constant water-mass formation rate Q, and that the freshwater flux and ocean salinity consist of a climatological value plus a time-dependent perturbation ($\bar{F}+F'$ and $\bar{s}+s'$, respectively). Then, (8) yields:

$$\rho V \frac{ds'}{dt} = \rho Q s_{sw} - \rho_{fw} s_{sw} \bar{F} - \rho Q \bar{s} - \rho_{fw} s_{sw} F' - \rho Q s'. \quad (11)$$

As the climatological fluxes are in steady state, the first three terms on the right side in (11) cancel according to (9), resulting in:

$$\rho V \frac{ds'}{dt} = -\rho_{fw} s_{sw} F' - \rho Q s'. \quad (12)$$

We approximated the freshwater-flux perturbation by our estimated trend ($F'=at$), and rearranged the terms resulting in a first order linear differential equation:

$$\frac{ds'}{dt} + \frac{Q}{V} s' = -\frac{\rho_{fw} s_{sw} a}{\rho V} t. \quad (13)$$

Integration in time yields an expression for the time-dependent evolution of the salinity perturbation:

$$s' = -\frac{\rho_{fw} s_{sw} a}{\rho Q} \left(t - \frac{V}{Q} + \frac{V}{Q} e^{-\frac{Q}{V} t} \right). \quad (14)$$

To obtain an estimate of the salinity trend at a given time *t*, we substituted (14) into (13):

$$\frac{ds'}{dt} = \frac{\rho_{fw} s_{sw} a}{\rho Q} \left(e^{-\frac{Q}{V} t} - 1 \right). \quad (15)$$

The equilibrium response of the system, i.e., the long-term trend after several years of perturbation is:

$$\lim_{t \to \infty} \frac{ds'}{dt} = -\frac{\rho_{fw} s_{sw} a}{\rho Q}. \quad (16)$$

Using our estimated sea-ice freshwater transport trend of +9±5 mSv per decade and a water-mass formation rate as above, we obtained an equilibrium freshening rate of −0.023±0.014 g kg^{-1} per decade (green in Extended Data Figure 7b), which is valid for sufficiently large *Qt/V*.

Extended Data Figure 7b (purple and blue; using 14) shows that if we assumed that the trend started in 1982, there would be a delayed response lowering the mean salinity trend estimate depending on *V*. We thus tested the sensitivity of the trend to *V*, which corresponds to the upper 150 m between the zero sea-ice-ocean freshwater flux line and the Subantarctic Front[79] (Extended Data Figure 7a), which is the source region of AAIW. The circumpolar *V* of about 5×10^6 km^3 results in a mean salinity trend (using 14) of −0.014±0.008 g kg^{-1} per decade between 1982 and 2008 (purple). However, AAIW formation does not occur in a circumpolar belt but mostly in the south-eastern Pacific and north-western Atlantic, i.e., on either side of Drake Passage[80–84]. Assuming that most of the water is modified in this region and further downstream in the South Pacific[80,82,84], we estimated a second, somewhat smaller *V* of about 2×10^6 km^3 (blue). The sea-ice freshwater transport trend into this reference volume is about +8±5 mSv per decade (Figures 2c-d), resulting in a mean salinity trend (using 14) of −0.018±0.010 g kg^{-1} per decade (blue). Since a certain amount of freshwater is transported eastward, out of this sector (blue), the mean trend of the delayed response lies somewhere in between the estimates based on the two different reference volumes (blue and purple).

It is unlikely that the trend started exactly in 1982. Thus, the actual salinity response will fall between our estimated delayed response and the equilibrium response. For the range of values

722 in the discussion above, the deviations of the freshening rate due to effects of delay and
723 variations in reference volume are much smaller than the actual magnitude of the trend itself.
724 We thus conclude that the overall mean freshening rate of newly formed AAIW and the surface
725 waters advected northward across the Subantarctic Front into SAMW due to the changes in sea-
726 ice freshwater transport is about -0.02 ± 0.01 g kg^{-1} per decade (Figure 1b).

31. Cavalieri, D. J. & Parkinson, C. L. Antarctic sea ice variability and trends, 1979–2006. *J. Geophys. Res.* **113,** C07004 (2008).
32. Comiso, J. C. Characteristics of Arctic winter sea ice from satellite multispectral microwave observations. *J. Geophys. Res.* **91,** 975–994 (1986).
33. Worby, A. P. *et al.* Thickness distribution of Antarctic sea ice. *J. Geophys. Res.* **113,** C05S92 (2008).
34. Schwegmann, S., Haas, C., Fowler, C. & Gerdes, R. A comparison of satellite-derived sea-ice motion with drifting-buoy data in the Weddell Sea, Antarctica. *Ann. Glaciol.* **52,** 103–110 (2011).
35. Kwok, R., Schweiger, A., Rothrock, D. A., Pang, S. & Kottmeier, C. Sea ice motion from satellite passive microwave imagery assessed with ERS SAR and buoy motions. *J. Geophys. Res.* **103,** 8191–8214 (1998).
36. Kwok, R. Ross sea ice motion, area flux, and deformation. *J. Clim.* **18,** 3759–3776 (2005).
37. CDO. Climate Data Operators (version 1.6.8). Available at: http://www.mpimet.mpg.de/cdo. (2015).
38. Comiso, J. C., Cavalieri, D. J., Parkinson, C. L. & Gloersen, P. Passive microwave algorithms for sea ice concentration: A comparison of two techniques. *Remote Sens. Environ.* **60,** 357–384 (1997).
39. Eisenman, I., Meier, W. N. & Norris, J. R. A spurious jump in the satellite record: has Antarctic sea ice expansion been overestimated? *Cryosphere* **8,** 1289–1296 (2014).
40. Kern, S. & Spreen, G. Uncertainties in Antarctic sea-ice thickness retrieval from ICESat. *Ann. Glaciol.* **56,** 107–119 (2015).
41. Kwok, R. & Maksym, T. Snow depth of the Weddell and Bellingshausen sea ice covers from IceBridge surveys in 2010 and 2011: An examination. *J. Geophys. Res. Ocean.* **119,** 4141–4167 (2014).
42. Williams, G. *et al.* Thick and deformed Antarctic sea ice mapped with autonomous underwater vehicles. *Nat. Geosci.* **8,** 61–67 (2015).
43. Yi, D., Zwally, H. J. & Robbins, J. W. ICESat observations of seasonal and interannual variations of sea-ice freeboard and estimated thickness in the Weddell Sea, Antarctica (2003-2009). *Annals of Glaciology* **52,** 43–51 (2011).
44. Kern, S., Ozsoy-Çiçek, B. & Worby, A. Antarctic sea-ice thickness retrieval from ICESat: Inter-comparison of different approaches. *Remote Sens.* **8,** 538 (2016).
45. Maksym, T. & Markus, T. Antarctic sea ice thickness and snow-to-ice conversion from atmospheric reanalysis and passive microwave snow depth. *J. Geophys. Res.* **113,** C02S12 (2008).
46. Zhang, J. Modeling the impact of wind intensification on Antarctic sea ice volume. *J. Clim.* **27,** 202–214 (2014).
47. Holland, P. R. *et al.* Modeled trends in Antarctic sea ice thickness. *J. Clim.* **27,** 3784–3801 (2014).
48. Emery, W. J., Fowler, C. W. & Maslanik, J. A. in *Oceanographic applications of remote sensing* (eds. Ikeda, M. & Dobson, F. W.) 367–379 (CRC Press, 1995).
49. Emery, W. J., Fowler, C. W. & Maslanik, J. A. Satellite-derived maps of Arctic and Antarctic sea ice motion: 1988 to 1994. *Geophys. Res. Lett.* **24,** 897–900 (1997).
50. Maslanik, J. *et al.* AVHRR-based Polar Pathfinder products for modeling applications. *Ann. Glaciol.* **25,** 388–392 (1997).
51. Heil, P., Fowler, C. W., Maslanik, J. A., Emery, W. J. & Allison, I. A comparison of East Antartic sea-ice motion derived using drifting buoys and remote sensing. *Ann. Glaciol.* **33,** 139–144 (2001).
52. Sumata, H. *et al.* An intercomparison of Arctic ice drift products to deduce uncertainty estimates. *J. Geophys. Res. Ocean.* **119,** 4887–4921 (2014).

53. Haumann, F. A. Dynamical interaction between atmosphere and sea ice in Antarctica. *Master's Thesis: Utrecht University* (Utrecht University, 2011).
54. Ohshima, K. I., Nakanowatari, T., Riser, S., Volkov, Y. & Wakatsuchi, M. Freshening and dense shelf water reduction in the Okhotsk Sea linked with sea ice decline. *Prog. Oceanogr.* **126,** 71–79 (2014).
55. Timco, G. W. & Frederking, R. M. W. A review of sea ice density. *Cold Reg. Sci. Technol.* **24,** 1–6 (1996).
56. Vancoppenolle, M., Fichefet, T. & Goosse, H. Simulating the mass balance and salinity of Arctic and Antarctic sea ice. 2. Importance of sea ice salinity variations. *Ocean Model.* **27,** 54–69 (2009).
57. Olason, E. & Notz, D. Drivers of variability in Arctic sea-ice drift speed. *J. Geophys. Res. Ocean.* **119,** 5755–5775 (2014).
58. Wentz, F. J. *User's manual: SSM/I antenna temperature tapes (revision 1), report number 120191*. (1991).
59. Thorndike, A. S. & Colony, R. Sea ice motion in response to geostrophic winds. *J. Geophys. Res.* **87,** 5845–5852 (1982).
60. Kimura, N. Sea ice motion in response to surface wind and ocean current in the Southern Ocean. *J. Meteorol. Soc. Japan* **82,** 1223–1231 (2004).
61. Peterson, T. C. *et al.* Homogeneity adjustments of in situ atmospheric climate data: a review. *Int. J. Climatol.* **18,** 1493–1517 (1998).
62. Aguilar, E., Auer, I., Brunet, M., Peterson, T. C. & Wieringa, J. *Guidelines on climate metadata and homogenization*. (WCDMP-53, WMO, 2003).
63. Santer, B. D. *et al.* Statistical significance of trends and trend differences in layer-average atmospheric temperature time series. *J. Geophys. Res.* **105,** 7337–7356 (2000).
64. Tamura, T., Ohshima, K. I. & Nihashi, S. Mapping of sea ice production for Antarctic coastal polynyas. *Geophys. Res. Lett.* **35,** L07606 (2008).
65. Ohshima, K. I. *et al.* Antarctic Bottom Water production by intense sea-ice formation in the Cape Darnley polynya. *Nat. Geosci.* **6,** 235–240 (2013).
66. Comiso, J. C., Kwok, R., Martin, S. & Gordon, A. L. Variability and trends in sea ice extent and ice production in the Ross Sea. *J. Geophys. Res.* **116,** C04021 (2011).
67. Martin, S., Drucker, R. S. & Kwok, R. The areas and ice production of the western and central Ross Sea polynyas, 1992-2002, and their relation to the B-15 and C-19 iceberg events of 2000 and 2002. *J. Mar. Syst.* **68,** 201–214 (2007).
68. Assmann, K. M. & Timmermann, R. Variability of dense water formation in the Ross Sea. *Ocean Dyn.* **55,** 68–87 (2005).
69. Timmermann, R., Beckmann, A. & Hellmer, H. H. The role of sea ice in the fresh-water budget of the Weddell Sea, Antarctica. *Ann. Glaciol.* **33,** 419–424 (2001).
70. Harms, S., Fahrbach, E. & Strass, V. H. Sea ice transports in the Weddell Sea. *J. Geophys. Res.* **106,** 9057–9073 (2001).
71. Kottmeier, C. & Sellmann, L. Atmospheric and oceanic forcing of Weddell Sea ice motion. *J. Geophys. Res. Ocean.* **101,** 20809–20824 (1996).
72. Ingleby, B. & Huddleston, M. Quality control of ocean temperature and salinity profiles — Historical and real-time data. *J. Mar. Syst.* **65,** 158–175 (2007).
73. Ren, L., Speer, K. & Chassignet, E. P. The mixed layer salinity budget and sea ice in the Southern Ocean. *J. Geophys. Res. Ocean.* **116,** C08031 (2011).
74. Jacobs, S. S. Bottom water production and its links with the thermohaline circulation. *Antarct. Sci.* **16,** 427–437 (2004).
75. Depoorter, M. A. *et al.* Calving fluxes and basal melt rates of Antarctic ice shelves. *Nature* **502,** 89–92 (2013).
76. Silva, T. A. M., Bigg, G. R. & Nicholls, K. W. Contribution of giant icebergs to the Southern Ocean freshwater flux. *J. Geophys. Res. Ocean.* **111,** C03004 (2006).

77. Jacobs, S. S., Fairbanks, R. G. & Horibe, Y. in *Oceanology of the Antarctic Continental Shelf* (ed. Jacobs, S. S.) 59–85 (American Geophysical Union, 1985). doi:10.1029/AR043p0059
78. Meredith, M. P. *et al.* Changes in the freshwater composition of the upper ocean west of the Antarctic Peninsula during the first decade of the 21st century. *Prog. Oceanogr.* **87,** 127–143 (2010).
79. Orsi, A. H., Whitworth, T. & Nowlin, W. D. On the meridional extent and fronts of the Antarctic Circumpolar Current. *Deep. Res. Part I* **42,** 641–673 (1995).
80. England, M. H., Godfrey, J. S., Hirst, A. C. & Tomczak, M. The mechanism for Antarctic Intermediate Water renewal in a world ocean model. *J. Phys. Oceanogr.* **23,** 1553–1560 (1993).
81. Talley, L. D. in *The South Atlantic: present and past circulation* (eds. Wefer, G., Berger, W. H., Siedler, G. & Webb, D. J.) 219–238 (Springer, 1996). doi:10.1007/978-3-642-80353-6_11
82. Iudicone, D., Rodgers, K. B., Schopp, R. & Madec, G. An exchange window for the injection of Antarctic Intermediate Water into the South Pacific. *J. Phys. Oceanogr.* **37,** 31–49 (2007).
83. Sloyan, B. M. & Rintoul, S. R. Circulation, renewal, and modification of Antarctic Mode and Intermediate Water. *J. Phys. Oceanogr.* **31,** 1005–1030 (2001).
84. Hartin, C. A. *et al.* Formation rates of Subantarctic mode water and Antarctic intermediate water within the South Pacific. *Deep. Res. Part I* **58,** 524–534 (2011).
85. Durack, P. J. & Wijffels, S. E. Fifty-year trends in global ocean salinities and their relationship to broad-scale warming. *J. Clim.* **23,** 4342–4362 (2010).

	Flux [mSv]	Δt [mSv]	ΔA [mSv]	Δc [mSv]	Δh [mSv]	Δu [mSv]	ΔC_{fw} [mSv]
Southern Ocean:							
Transport	+130 ±30	±0	±5	±0	±16	±25	±6
Net open ocean	+130 ±30	±0	±5	±0	±16	±25	±6
Net coastal ocean	-130 ±30	±0	±5	±0	±14	±26	±6
Net continental shelf	-60 ±20	±0	±0	±0	±8	±13	±3
Total melting	+460 ±100	±37	-	±1	±74	±49	±23
Total freezing	−410 ±110	±37	-	±1	±73	±50	±23
Atlantic sector:							
Transport	+60 ±20	±0	±1	±0	±13	±11	±3
Net open ocean	+60 ±20	±0	±1	±0	±13	±11	±3
Net coastal ocean	-50 ±20	±0	±1	±0	±14	±9	±3
Net continental shelf	-20 ±5	±0	±0	±0	±2	±4	±1
Total melting	+180 ±40	±13	-	±0	±25	±21	±9
Total freezing	−160 ±40	±13	-	±0	±25	±19	±9
Indian Ocean sector:							
Transport	+10 ±5	±0	±1	±0	±4	±2	±1
Net open ocean	+10 ±5	±0	±1	±0	±4	±2	±1
Net coastal ocean	-10 ±6	±0	±1	±0	±4	±4	±1
Net continental shelf	-10 ±4	±0	±0	±0	±3	±2	±0
Total melting	+70 ±30	±7	-	±0	±24	±5	±4
Total freezing	−70 ±30	±7	-	±0	±24	±6	±4
Pacific sector:							
Transport	+60 ±20	±0	±2	±0	±9	±12	±3
Net open ocean	+60 ±20	±0	±2	±0	±9	±12	±3
Net coastal ocean	-60 ±20	±0	±2	±0	±9	±13	±3
Net continental shelf	-30 ±9	±0	±0	±0	±6	±6	±2
Total melting	+200 ±50	±17	-	±0	±43	±23	±10
Total freezing	−180 ±60	±17	-	±0	±43	±24	±10

Extended Data Table 1 | Mean and uncertainties of annual sea-ice freshwater fluxes over the period 1982 through 2008. Positive numbers indicate a freshwater flux into the ocean or northward transport (1 mSv = 10^3 m^3 s^{-1}). The final uncertainty estimate (95% confidence level) stems from the uncertainties in the filtering of high-frequency temporal noise (Δt), variations of the zero freshwater flux line (ΔA), sea-ice concentration (Δc), sea-ice thickness (Δh), sea-ice drift (Δu), and the freshwater conversion factor (ΔC_{fw}), respectively. See Methods for details. See Figure 2 for definition of regions.

	Flux [mSv dec^{-1}]	Δs_e [mSv dec^{-1}]	Δt [mSv dec^{-1}]	ΔA [mSv dec^{-1}]	Δc [mSv dec^{-1}]	Δh [mSv dec^{-1}]	Δu [mSv dec^{-1}]	ΔC_{fw} [mSv dec^{-1}]
Southern Ocean:								
Transport	**+9** ±5	±3.2	±0.3	±1.1	±0.8	±3.0	±1.9	±0.5
Net open ocean	**+10** ±5	±3.5	±0.4	±1.1	±0.8	±3.0	±2.0	±0.5
Net coastal ocean	**-10** ±5	±3.5	±0.2	±1.1	±0.7	±3.3	±1.1	±0.5
Net continental shelf	**-3** ±2	±1.8	±0.0	±0.0	±0.1	±0.8	±0.1	±0.1
Atlantic sector:								
Transport	-4 ±5	±4.3	±0.1	±0.7	±0.1	±1.4	±0.7	±0.2
Net open ocean	-4 ±5	±4.4	±0.1	±0.7	±0.1	±1.4	±0.7	±0.2
Net coastal ocean	+6 ±6	±5.7	±0.1	±0.7	±0.0	±0.6	±1.8	±0.3
Net continental shelf	**+6** ±3	±2.5	±0.0	±0.0	±0.0	±0.6	±1.6	±0.3
Indian Ocean sector:								
Transport	-1 ±1	±1.3	±0.0	±0.2	±0.1	±0.3	±0.2	±0.0
Net open ocean	-1 ±1	±1.3	±0.0	±0.2	±0.1	±0.3	±0.2	±0.0
Net coastal ocean	**-3** ±2	±0.9	±0.0	±0.2	±0.1	±1.1	±0.7	±0.1
Net continental shelf	**+2** ±1	±0.9	±0.1	±0.0	±0.1	±0.3	±0.4	±0.1
Pacific sector:								
Transport	**+14** ±5	±3.4	±0.2	±0.6	±0.7	±1.3	±2.8	±0.7
Net open ocean	**+14** ±5	±3.4	±0.3	±0.5	±0.7	±1.2	±2.9	±0.7
Net coastal ocean	**-13** ±5	±3.6	±0.2	±0.5	±0.6	±1.9	±2.3	±0.7
Net continental shelf	**-10** ±3	±2.6	±0.1	±0.0	±0.2	±1.2	±1.8	±0.5

Extended Data Table 2 | Decadal trends of annual sea-ice freshwater fluxes and their uncertainties over the period 1982 through 2008. Positive numbers indicate a freshwater flux trend into the ocean or a northward transport trend (1 mSv dec^{-1} = 10^3 m^3 s^{-1} per decade). The final uncertainty estimate (95% confidence level) stems from the standard error of the slope of the regression line (Δs_e), filtering of high-frequency temporal noise (Δt), variations of the zero freshwater flux line (ΔA), sea-ice concentration (Δc), sea-ice thickness (Δh), sea-ice drift (Δu), and the freshwater conversion factor (ΔC_{fw}), respectively. Bold numbers indicate a significance of at least a 90% confidence level. See Methods for details. See Figure 2 for definition of regions.

	Southern Ocean	Atlantic sector	Indian Ocean sector	Pacific sector
1992 – 2004: Flux trend [mSv dec^{-1}]	+4 ±9	-12 ±11	**-5** ±3	**+21** ±10
1992 – 2008: Flux trend [mSv dec^{-1}]	**+11** ±8	-5 ±9	-2 ±2	**+17** ±8
1982 – 2004: Flux trend [mSv dec^{-1}]	**+8** ±5	-6 ±5	-1 ±1	**+15** ±6
1982 – 2008: Flux trend [mSv dec^{-1}]	**+9** ±5	-4 ±5	-1 ±1	**+14** ±5
1982 – 2008 Monte Carlo analysis:				
Flux offset before 1987 [mSv]	+19 ±5	+13 ±7	+3 ±2	+4 ±5
Probability for trend of same sign [%]	100	92	78	100
Probability for significant trend of same sign [%]	92	26	9	100
Posterior trend uncertainty [mSv dec^{-1}]	±5	±6	±2	±5

Extended Data Table 3 | Sensitivity of northward sea-ice freshwater transport trend to time periods and homogenisation. Positive numbers indicate a northward freshwater transport trend (1 mSv dec^{-1} = 10^3 m^3 s^{-1} per decade). Bold numbers indicate a significance of the trend of at least a 90% confidence level. The Monte Carlo analysis is performed for 10^4 normally distributed sample offsets. Uncertainties (95% confidence level) stem from the standard error of the slope of the regression line and the data uncertainty. See Methods for details. See Figure 2 for definition of regions.

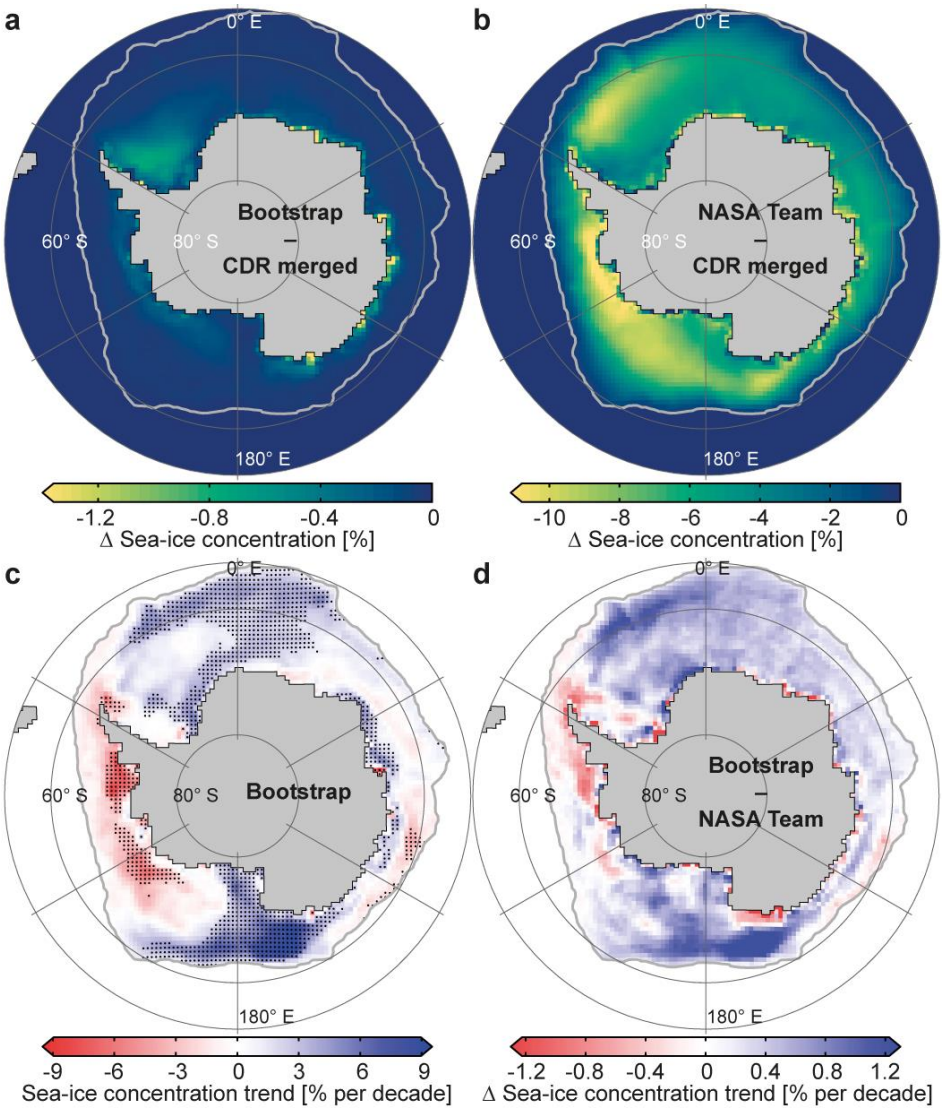

878

879 **Extended Data Figure 1 | Uncertainties and trends in Antarctic sea-ice concentration over**
880 **the period 1982 through 2008. a,** Bootstrap (BA) minus CDR merged data. **b,** NASA Team
881 (NTA) minus CDR merged data. **c,** Decadal trends of the BA sea-ice concentration. Stippled
882 trends are statistically significant (at least 90% level). **d,** Decadal trends of Bootstrap minus
883 NASA Team data. The thick grey line marks the mean sea-ice edge (1% sea-ice concentration).
884 See Methods for details.

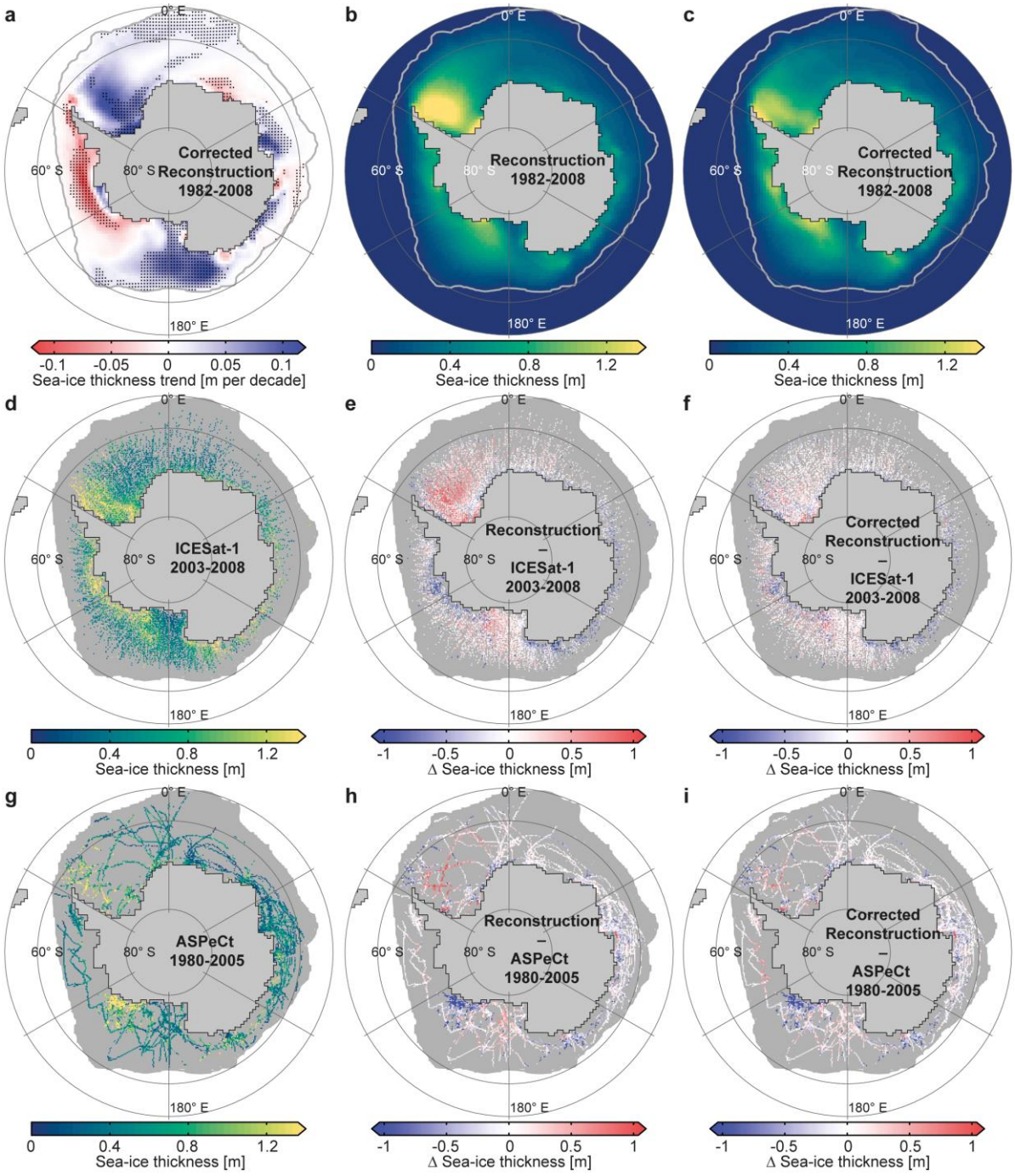

Extended Data Figure 2 | Mean, trend, and uncertainty of Antarctic sea-ice thickness. a, Decadal trends of the corrected reconstruction (1982-2008). Stippled trends are statistically significant (at least 90% level). **b,** Mean of the reconstruction (1982-2008). **c,** Mean of the corrected reconstruction (1982-2008). **d,** Mean of the non-gridded ICESat-1 data (2003-2008, 13 campaigns). **e,** Reconstruction minus non-gridded ICESat-1 data (2003-2008). **f,** Corrected reconstruction minus non-gridded ICESat-1 data (2003-2008). **g,** Mean of the ASPeCt data (1980-2005). **h,** Reconstruction minus ASPeCt data (1980-2005). **i,** Corrected reconstructions minus ASPeCt data (1980-2005). The thick grey line marks the mean sea-ice edge (1% sea-ice concentration). Differences are based on data when both respective products were available. Data points without data in the sea-ice covered region are grey shaded in d-i. See Methods for details.

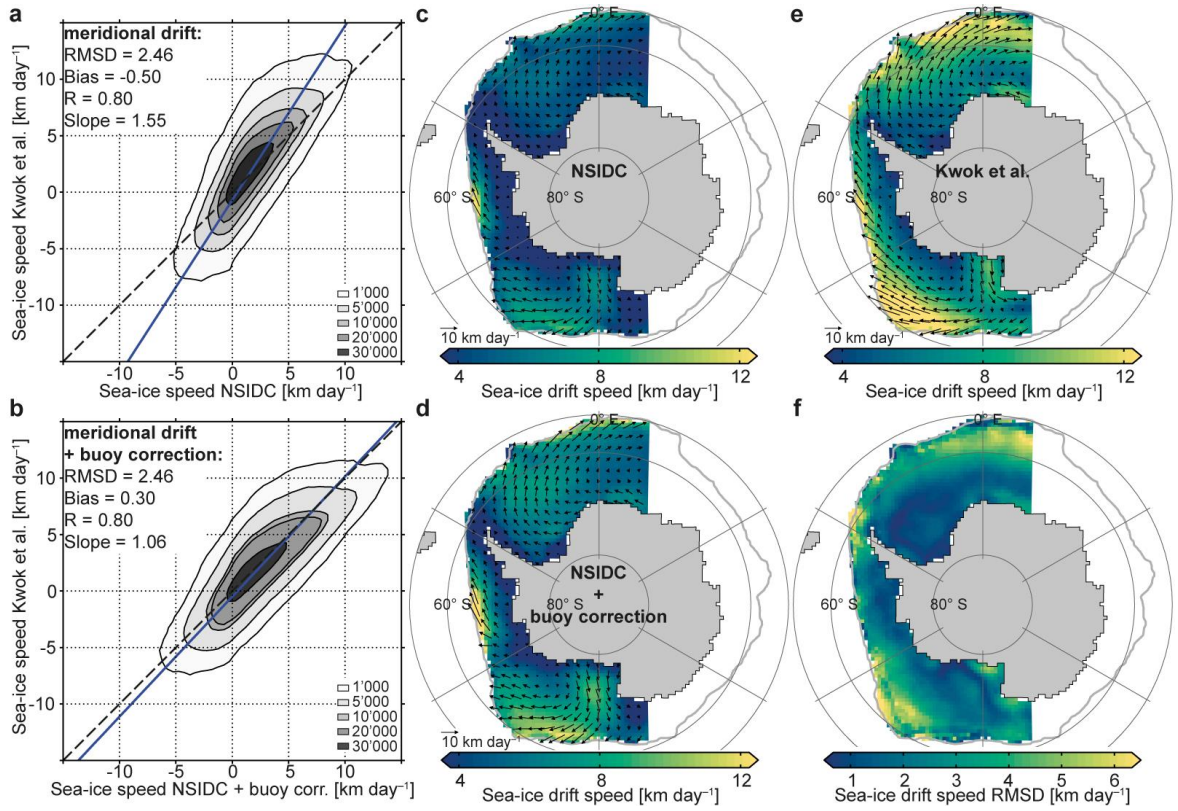

Extended Data Figure 3 | Sea-ice drift speed comparison between the NSIDC and Kwok et al. data for the period 1992 to 2003. a-b, Low-pass filtered, 21-day running mean, (a) original and (b) bias-corrected daily meridional NSIDC sea-ice drift speed compared to the low-pass filtered daily meridional Kwok et al. data. Contours mark the number of grid boxes and the blue line marks the fitted least squares linear regression line. **c-e,** Mean sea-ice drift speed of the (c) original and (d) bias-corrected NSIDC, and (e) Kwok et al. sea-ice drift speed. Arrows denote the drift vectors. **f,** Root-mean-square differences between the annual mean bias-corrected NSIDC and Kwok et al. sea-ice drift speed. The thick grey line in c-f marks the mean sea-ice edge (1% sea-ice concentration). Data points were compared when both data sets were available. See Methods for details.

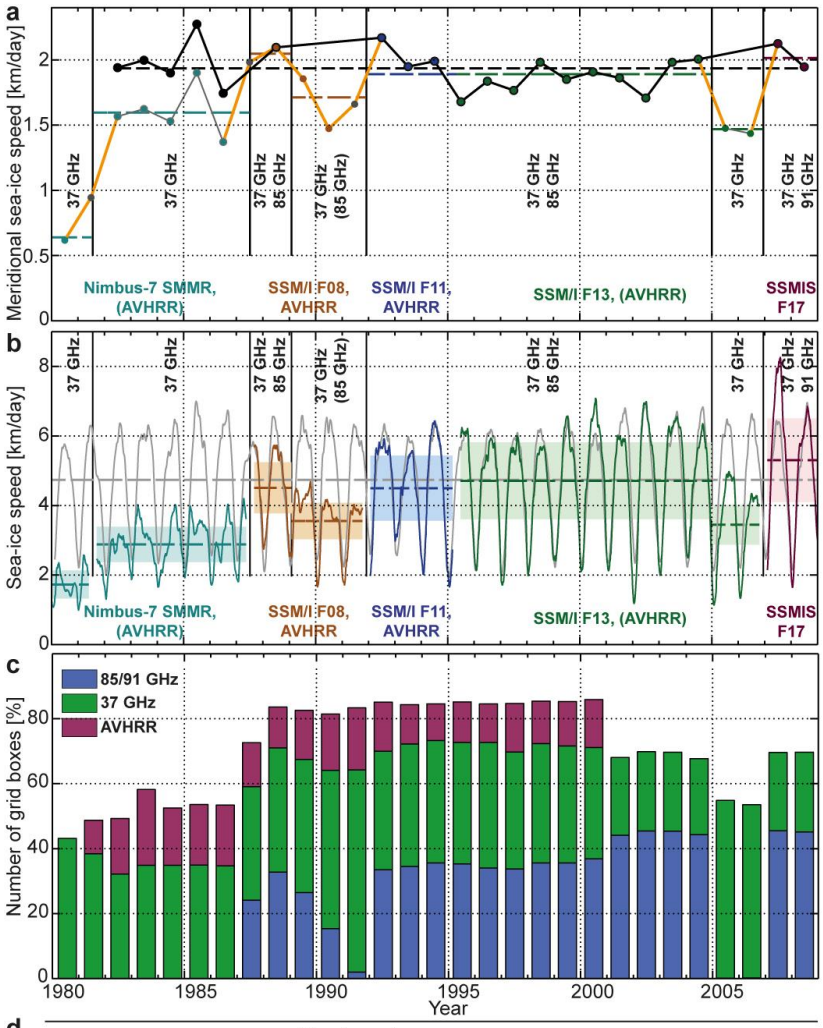

d

Instruments	Passive microwave sensor channels	Start date	End date
Nimbus-7 SMMR	37 GHz	01.01.1980	23.07.1981
Nimbus-7 SMMR, AVHRR	37 GHz	24.07.1981	08.07.1987
SSM/I F08, AVHRR	37 GHz, 85 GHz	09.07.1987	31.01.1989
SSM/I F08, AVHRR	37 GHz, 85 GHz degrading	01.02.1989	02.12.1991
SSM/I F11, AVHRR	37 GHz, 85 GHz	03.12.1991	02.05.1995
SSM/I F13, AVHRR	37 GHz, 85 GHz	03.05.1995	30.12.2000
SSM/I F13	37 GHz, 85 GHz	31.12.2000	31.12.2004
SSM/I F13	37 GHz	01.01.2005	13.12.2006
SSMIS F17	37 GHz, 91 GHz	14.12.2006	31.12.2008

Extended Data Figure 4 | Temporal inhomogeneities in the NSIDC satellite sea-ice drift data. a, Annual mean meridional sea-ice drift speed averaged over the entire sea-ice area (sea-ice concentration >50%). Thick orange lines: spurious trends due to changes in underlying data; black: data corrected for inconsistencies and used in this study (1982 to 2008). **b,** Low-pass filtered (91-day running mean) sea-ice drift speed averaged over the entire sea-ice area (sea-ice concentration >50%). Grey: reduced wind speed from ERA-Interim using a reduction factor from the period 1988 to 2008. (a-b) In colour: uncorrected data for each respective underlying satellite instrument combination; dashed lines: mean over the respective period; black vertical lines: periods of the same underlying channels. Text denotes the sensors and the frequency of the microwave radiometer channels used. **c,** Fraction of sea-ice covered grid boxes with at least one drift vector observation in a 21-day window and a 75 by 75 km grid box using the non-gridded NSIDC drift data. Colours indicate the contribution of each sensor and channel. **d,** Different combinations of instruments and passive microwave sensor channels and the related periods underlying the NSIDC sea-ice drift data. See Methods for details.

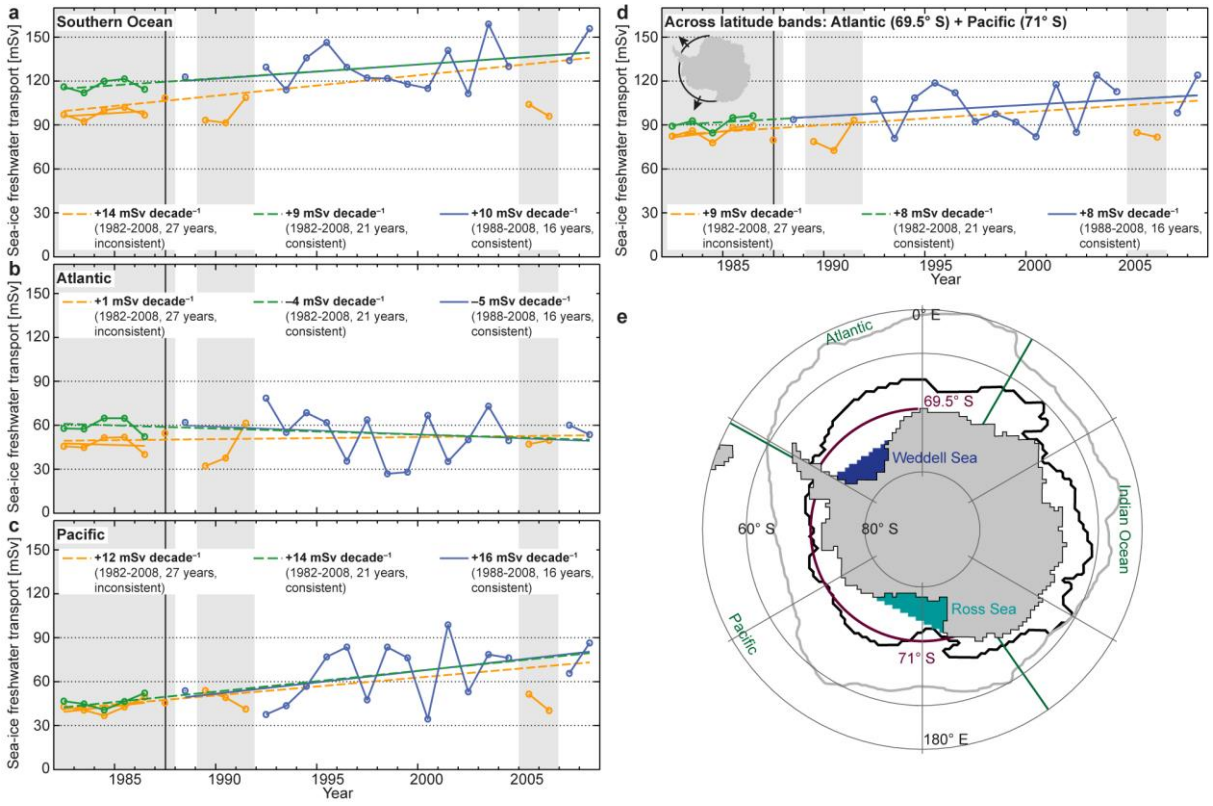

Extended Data Figure 5 | Time series and regions of annual northward sea-ice freshwater transport. Transport from the coastal ocean to the open ocean region in the (**a**) Southern Ocean (**b**) Atlantic sector (**c**) Pacific sector. **d,** Across latitude bands in the Atlantic (69.5° S) and Pacific (71° S) sectors. Orange: not accounting for inhomogeneities; blue: homogeneous years only; green: homogenised time series. Corrected or removed years are shaded in grey. Straight lines show the linear regressions for the periods 1982 to 2008 (dashed orange and green), 1982 to 1986 (solid orange), and 1988 to 2008 (homogeneous years only; solid blue). See Methods for details. **e,** Regions used for evaluation of the sea-ice freshwater fluxes. Turquoise shading: area south of the coastal Ross Sea flux gate[13,36,66]; dark blue shading: area south of the coastal Weddell Sea flux gate[13]; purple lines: 69.5° S latitude band in the Atlantic sector and 71° S latitude band in the Pacific sector; black line: smoothed mean zero sea-ice-ocean freshwater flux line dividing the coastal and open ocean regions (see Methods); thick grey line: mean sea-ice edge (1% sea-ice concentration); green lines: basin boundaries.

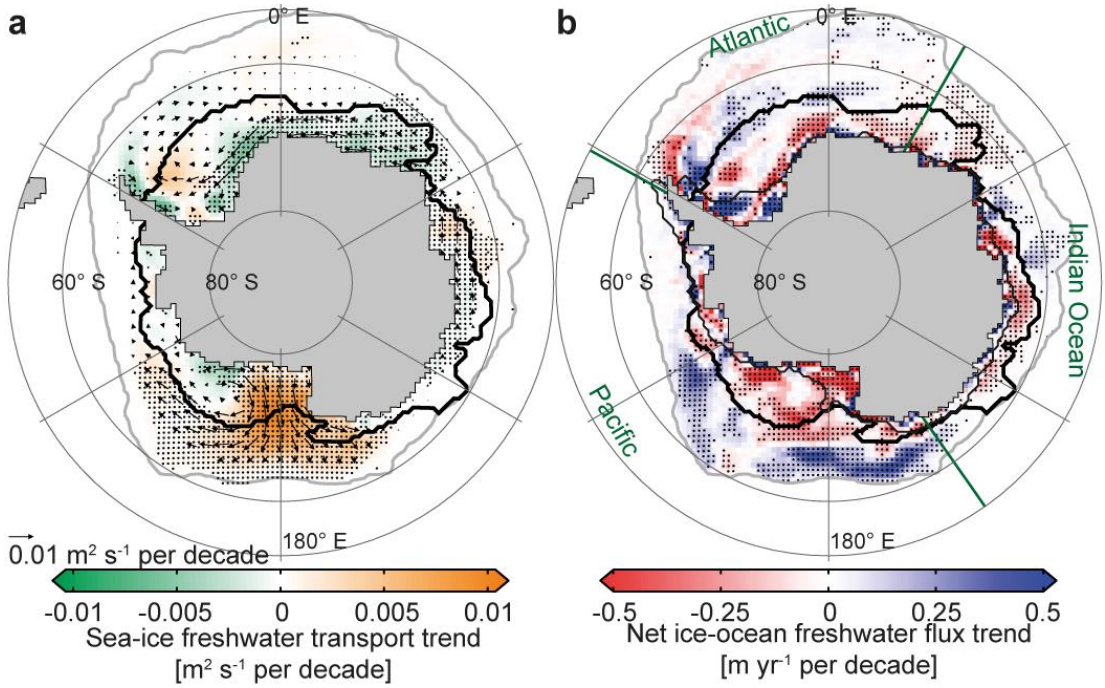

937

938 **Extended Data Figure 6 | Trends of net annual freshwater fluxes associated with sea ice**
939 **over the period 1982 through 2008 if temporal inhomogeneities in the sea-ice drift data**
940 **were not considered.** Linear trends of (a) meridional sea-ice freshwater transport and (b) net
941 sea-ice-ocean freshwater flux from freezing and melting. Arrows (a) denote the trend of the
942 annual transport vectors. Stippled trends are significant at the 90% level (Methods). Thick black
943 lines: zero sea-ice-ocean freshwater flux line used to divide the coastal from the open ocean
944 regions; thin black lines: continental shelf (1000-m isobath); grey lines: sea-ice edge (1% sea-
945 ice concentration); green lines: basin boundaries.

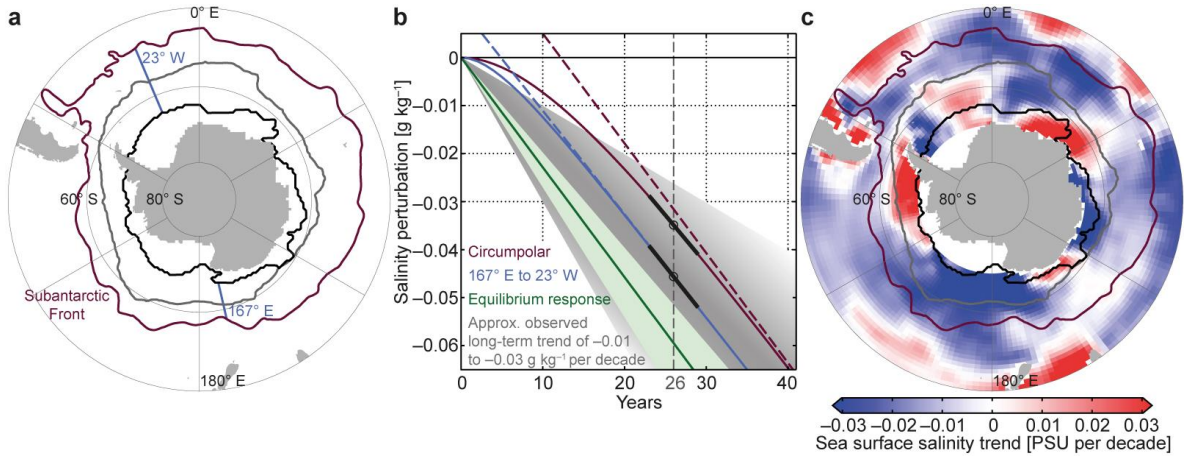

946

947 **Extended Data Figure 7 | Contribution of sea-ice freshwater flux trends to ocean salinity.**
948 **a,** Map showing the regions used for the estimation of salinity changes due to sea-ice freshwater
949 fluxes. Blue lines: sector important for AAIW formation (167° E to 23° W); purple line:
950 Subantarctic Front[79]; black line: smoothed mean zero freshwater flux line dividing the coastal
951 and open ocean regions; thick grey line: mean sea-ice edge (1% sea-ice concentration). **b,**
952 Salinity response to a freshwater flux perturbation using the long-term equilibrium response
953 (green) and using a delayed response starting in 1982 for a circumpolar reference volume
954 (5×10^6 km^3; purple), or for the region of most AAIW formation (2×10^6 km^3; blue). See Methods
955 for details. Dashed lines: respective asymptotic equilibrium response; black lines: respective
956 current trends; grey shading: approximate observed long-term trend in AAIW[1,3,4]. **c,** Observed
957 long-term sea-surface salinity trends (data from P. Durack & S. Wijffels,
958 http://www.cmar.csiro.au/oceanchange; 1950 to 2000)[5,85].